HHS Public Access

Author manuscript

Cell. Author manuscript; available in PMC 2024 July 20.

Published in final edited form as:

Cell. 2023 July 20; 186(15): 3208–3226.e27. doi:10.1016/j.cell.2023.05.047.

QKI shuttles internal m^{7}G-modified transcripts into stress granules and modulates mRNA metabolism

Zhicong Zhao[1,2,9], **Ying Qing**[1,9], **Lei Dong**[1,9], **Li Han**[1,4], **Dong Wu**[1], **Yangchan Li**[1,5], **Wei Li**[1], **Jianhuang Xue**[1,6,7], **Keren Zhou**[1], **Miao Sun**[8], **Brandon Tan**[1], **Zhenhua Chen**[1], **Chao Shen**[1], **Lei Gao**[1], **Andrew Small**[1], **Kitty Wang**[1], **Keith Leung**[1], **Zheng Zhang**[1], **Xi Qin**[1], **Xiaolan Deng**[1], **Qiang Xia**[2,*], **Rui Su**[1,*], **Jianjun Chen**[1,3,10,*]

[1]Department of Systems Biology, Beckman Research Institute of City of Hope, Monrovia, CA 91016, USA

[2]Department of Liver Surgery, Renji Hospital, School of Medicine, Shanghai Jiao Tong University, Shanghai 200127, China

[3]City of Hope Comprehensive Cancer Center, City of Hope, Duarte, CA 91010, USA

[4]School of Pharmacy, China Medical University, Shenyang, Liaoning 110001, China

[5]Department of Radiation Oncology, The First Affiliated Hospital of Sun Yat-sen University, Guangzhou, Guangdong 510080, China

[6]Key Laboratory of Spine and Spinal Cord Injury Repair and Regeneration of Ministry of Education, Tongji Hospital affiliated to Tongji University, Shanghai, 200065, China

[7]Frontier Science Center for Stem Cell Research, School of Life Sciences and Technology, Tongji University, Shanghai, 200092, China

[8]Keck School of Medicine, University of Southern California, and Department of Pathology and Laboratory Medicine, Children's Hospital Los Angeles, Los Angeles, CA 90033, USA

[9]These authors contributed equally

[10]Lead contact

Summary

N^7-methylguanosine (m^{7}G) modification, routinely occurring at mRNA 5' cap or within tRNAs/rRNAs, also exists internally in messenger RNAs (mRNAs). While m^{7}G-cap is essential for pre-mRNA processing and protein synthesis, the exact role of mRNA internal m^{7}G modification

*Correspondence: jianchen@coh.org (J.C.), rsu@coh.org (R.S.) and xiaqiang@shsmu.edu.cn (Q.X.).

Author contributions

Conceptualization and supervision, R.S. and J.C.; methodology, Z. Zhao; formal analysis, L.D. and K.Z.; investigation, Z. Zhao, Y.Q., L.H., D.W., W.L., J.X., Y.L., M.S., B.T., Z.C., C.S., Z. Zhang, X.Q., K.W., K.L., A.S., and X.D.; funding acquisition, B.T., R.S. and J.C.; writing – original draft, Z. Zhao, L.D., Y.Q. and R.S.; writing – review & editing, Z. Zhao, L.D., Y.Q., Q.X., R.S., and J.C.

Declaration of interests

The authors declare no competing interests.

remains elusive. Here, we report that mRNA internal m^{7}G is selectively recognized by Quaking proteins (QKIs). Via transcriptome-wide profiling/mapping of internal m^{7}G methylome and QKI binding sites, we identified over 1,000 high-confidence m^{7}G-modified and QKI-bound mRNA targets with a conserved "GANGAN (N = A/C/U/G)" motif. Strikingly, QKI7 interacts (via C-terminus) with the stress granule (SG) core protein G3BP1 and shuttles internal m^{7}G-modified transcripts into SGs to regulate mRNA stability and translation under stress conditions. Specifically, QKI7 attenuates the translation efficiency of essential genes in Hippo signaling pathway to sensitize cancer cells to chemotherapy. Collectively, we characterized QKIs as mRNA internal m^{7}G binding proteins that modulate target mRNA metabolism and cellular drug resistance.

Graphical Abstract

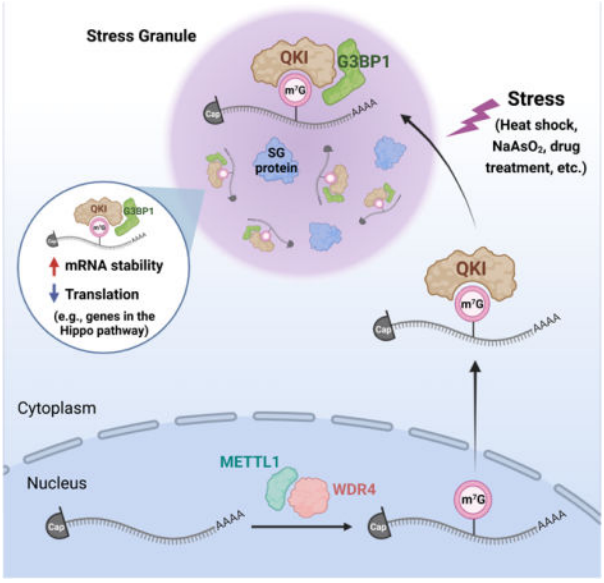

In Brief:

The Quaking protein QKI7 binds to internal m^{7}G-modified mRNAs and directs them to stress granules to suppress their translation under stress conditions.

Introduction

Analogous to DNA and histones, eukaryotic RNAs are also decorated with various chemical decorations, termed epitranscriptomics. Over 170 types of chemical modifications have been identified in almost all kinds of cellular RNAs, including mRNAs, transfer RNAs (tRNAs), ribosomal RNAs (rRNAs), and small nuclear RNAs (snRNAs).[1–3] In eukaryotic mRNAs, N^6-methyladenosine (m^{6}A) is the most prevalent internal modification. Characterization of m^{6}A machinery has revealed its profound roles in determining mRNA fates during normal development and pathological processes.[2,3] Besides m^{6}A, mRNAs also commonly contain m^{7}G (Figure 1A), another positively charged decoration ubiquitously located at the 5' extremity of mRNAs.[4] The m^{7}G-cap, catalyzed by RNA guanine-7 methyltransferase

during transcription initiation,[5] protects mRNAs from exonucleolytic decay and modulates pre-mRNA splicing and mRNA translation.[6] Meanwhile, tRNAs[7] and rRNAs[8] are also heavily m^7G-modified. The methyltransferase 1-WD repeat-containing protein 4 (METTL1-WDR4) complex deposits m^7G mark at position 46 (m^7G_{46}) of human tRNA loops to stabilize tRNAs and regulate translation efficiency.[9] METTL1-WDR4-mediated m^7G in tRNAs also attenuates ribosome pausing, potentiates mRNA translation, regulates the self-renewal and differentiation of embryonic stem cells, and facilitates tumor progression.[7,10,11] The m^7G mark at position 1639 (m^7G_{1639}) of human 18S rRNA is involved in pre-18S rRNA processing and 40S ribosomal subunit maturation.[12] Moreover, certain microRNAs (miRNAs), such as *let-7e*, are m^7G-methylated by METTL1 in human cancer cells, which is essential for miRNA maturation and secondary structure maintenance.[13]

Evidence is emerging that m^7G modification also exists internally within mRNAs as detected by distinct approaches, including enzyme treatment coupled with liquid chromatography-tandem mass spectrometry (LC-MS/MS),[14] m^7G-methylated RNA immunoprecipitation sequencing (MeRIP-seq), chemical-assisted m^7G sequencing,[15] m^7G mutational profiling sequencing,[16] and m^7G individual-nucleotide-resolution cross-linking and immunoprecipitation with sequencing (miCLIP-seq).[17] Based on current data, the internal mRNA m^7G/G level ranges from 0.02% to 0.05% in eukaryotes, which is 5% −10% of the m^6A/A ratio within mRNAs.[17,18] High-throughput sequencing reveals that it is enriched at 5’ UTR and GA-rich contexts across different human/mouse tissues and cell lines.[17] Notably, a cell-free RNA methylation assay suggests that the METTL1-WDR4 complex might be responsible for installing m^7G internally in mRNAs.[18] However, the biological functions of internal mRNA m^7G modifications have yet to be investigated, mainly due to the lack of identification of specific internal m^7G-binding protein(s) (also called “reader(s)”) that mediate(s) their functions. Therefore, it is critical to identify the specific binding protein(s) of mRNA internal m^7G modification.

The mRNA internal m^7G modification might be dynamic because its abundance and distribution across mRNAs are regulated under stress conditions.[17] Stress granules (SGs), the cytoplasmic membraneless organelles, are assembled under stress conditions to modulate mRNA storage, stability, and translation, and might be associated with tumorigenesis and drug resistance.[19–21] Recent studies suggest that RNAs and RNA-binding proteins (RBPs) are crucial components of SGs. The m^6A-binding YTHDF proteins recruit m^6A-modified mRNAs into SGs and promote phase separation and SG formation.[22–24] Whereas mRNA internal m^7G was reported to be important in mRNA metabolism under stress conditions,[17] little is known if stress affects the enrichment of internal m^7G-modified mRNAs in SGs and if so, what the biological consequence could be.

Here, through multiple high-throughput sequencing approaches and subsequent validation, we report a significant finding that Quaking proteins (QKIs) preferentially recognize internal mRNA m^7G modifications. QKI belongs to the STAR (signal transduction and activation of RNA metabolism) family of RBPs with K Homology (KH) domain.[25] The *QKI* gene encodes three major isoforms: QKI5, QKI6, and QKI7.[26] Consistent with previous reports,[27–29] we found that QKI6 and QKI7 are preferentially located in the cytoplasm, whereas QKI5 is predominantly located in the nucleus. Under stress conditions, QKI6 and

QKI7 directly interact with the SG core protein G3BP1, colocalize within SGs, shuttle hundreds of internal m^7G-modified mRNAs into SGs, and thereby affect mRNA stability and/or translation efficiency. The m^7G-modified mRNAs are enriched in the cytosol, especially SGs. *QKI* depletion abrogates the recruitment of m^7G-modified mRNAs into SGs in an m^7G-dependent manner. Moreover, QKI7 sensitizes cancer cells to chemotherapy drugs by suppressing the Hippo signaling pathway via an m^7G-dependent mechanism.

Results

Internal m^7G modification is enriched in the cytosolic mRNAs

We analyzed m^7G abundance via LC-MS/MS in different types of RNAs, including total RNA, small RNA (17–200 nt), rRNA, cap-depleted polyA$^+$ mRNA, cytoplasmic cap-depleted polyA$^+$ mRNA, and nuclear cap-depleted polyA$^+$ mRNA from HeLa and HepG2 cells (Figures S1A–S1C). After removing the 5' caps,[17] the m^7G abundance in mRNAs decreased dramatically (Figure S1D), suggesting the efficient removal of m^7G Cap. In both cell types, the m^7G/G level was approximately 0.1% in total RNAs, 1% in small RNAs (mainly tRNAs), and 0.03% in rRNAs and cap-depleted polyA$^+$ mRNAs (Figure 1B). Strikingly, cytoplasmic mRNAs had a significantly higher internal m^7G/G level than nuclear mRNAs in both cell types (Figures 1C, S1E, and S1F), implying a potential role of internal m^7G modification in cytoplasmic mRNA metabolism.

The METTL1-WDR4 complex is known to deposit m^7G in tRNAs and miRNAs,[7,30] and recent studies suggest it might also methylate a subset of internal m^7G sites in mRNAs.[17,18] We found that *METTL1* or *WDR4* depletion significantly decreased m^7G abundance in both small RNAs and cap-depleted polyA$^+$ mRNAs (Figures 1D–1G). Conversely, overexpression of wild-type METTL1, but not the catalytically inactive (EIR/AAA, amino acids 107–109) METTL1,[13] significantly increased the m^7G/G level in small RNAs and cap-depleted polyA$^+$ mRNAs; overexpression of WDR4 also evidently increased internal m^7G modification (Figures 1H–1J). The predominant nuclear localization of METTL1 and WDR4 suggests that mRNA internal m^7G modification is mainly deposited in the nucleus before m^7G-modified mRNAs are exported to the cytosol (Figure S1G).

It has been reported that mRNA internal m^7G promotes translation of target genes, such as *PCNA*, under stress conditions,[17] and that METTL1-mediated tRNA m^7G promotes tumor progression by enhancing global translation efficiency.[10,11] However, other studies showed that *METTL1* depletion did not affect overall mRNA translation levels, albeit probably affecting the translation efficiency of a subset of target transcripts.[13,18] Consistent with the latter reports, we found *METTL1* knockout (KO) did not substantially attenuate global translation efficiency in HepG2 and HeLa cells (Figures S1H–S1J).

Identification of QKIs as internal mRNA m^7G-binding protein

To identify the proteins directly binding to internal m^7G modification, we employed RNA affinity chromatography using internal m^7G-modified oligo bait or unmodified control coupled with mass spectrometry for an unbiased screen. Given that m^7G-modified RNA oligos are not commercially available, we synthesized two 60-mer oligos with either

GTP or m^7GTP as unique sources for a single G site (Figures 2A and 2B).[17,18] The mass spectrometry results showed that several proteins were selectively enriched in m^7G-containing RNA/protein complexes, but not G-containing complexes (Figure 2C and Table S2). Further RNA pulldown assay confirmed that the proteins enriched by m^7G bait, such as leucine rich pentatricopeptide repeat containing (LRPPRC), insulin like growth factor 2 mRNA binding protein 1 (IGF2BP1) and QKI, indeed showed much higher binding ability to internal m^7G-modified linear RNA (Figures 2D, 2E, and S2A).

To further characterize the genuine internal m^7G-binding protein(s), we analyzed motifs of METTL1, IGF2BP1, LRPPRC and QKI using public PAR-CLIP sequencing datasets.[31] Since mRNA internal m^7G is reported to be enriched in a GA-rich context,[17,18] we presumed that its methyltransferase METTL1 and *bona fide* binding protein(s) should preferentially bind to GA-rich motifs. As expected, the top motif for METTL1 was the GA-rich motif, “UGAAGA” (Figure 2F, left). Intriguingly, QKI also recognizes a “GA-rich” motif, “GAUGAU” (Figure 2F, right). However, no GA-rich motif was enriched for the binding sites of either IGF2BP1 or LRPPRC (Figure S2B). LRPPRC plays an essential in mitochondrial RNA metabolism[32,33] and is mainly distributed in mitochondria (Figure S2C). Considering that internal m^7G modification is not enriched in mitochondrial mRNA (Figure S2D) and top motifs of IGF2BP1 and LRPPRC binding sites do not contain the conserved m^7G motif, we excluded them from our further studies and mainly focused on QKI proteins. Our cell-free RNA pulldown assay showed that all three recombinant QKI proteins, QKI5, QKI6 and QKI7, preferentially bound to m^7G-modified oligonucleotides over unmodified ones (Figure 2G). QKI proteins also specially recognized m^7G-modified oligonucleotides *ex vivo* (Figures 2H and S2E). Consistently, both cell-free RNA immunoprecipitation (RIP) assay and *ex vivo* RIP assay demonstrated the significant enrichment of internal m^7G in QKI5/6/7-bound mRNAs (Figures 2I and 2J). The electrophoretic mobility shift assay (EMSA) further verified that QKI preferentially bound to m^7G-methylated RNAs (Figure S2F). Collectively, these results suggest QKIs selectively recognize internal m^7G-modified RNAs.

We next profiled the mRNA internal m^7G methylome with m^7G MeRIP-seq and characterized QKIs’ transcriptome-wide binding sites with RIP-seq in HepG2 cells. The m^7G MeRIP-seq with cap-depleted mRNAs[18] showed that m^7G peaks were enriched at start codon regions (Figure 2K), and a “GANGAN (N = A/C/U/G)” motif was significantly enriched in m^7G peaks (Figure 2L), consistent with previously reported internal m^7G motifs[17,18] and METTL1 motif (see Figure 2F, left). Internal m^7G modifications were identified in >3,000 transcripts and 61.3% (2,263/3,689) of them overlapped with another independent m^7G MeRIP-seq dataset from HepG2 cells (Figure S2G).[18] The 2,263 transcripts were thereby considered high-confidence internal m^7G targets (Table S3) and the majority of them overlapped with published QKI eCLIP-seq data[34] (Figure S2H). Through QKI RIP-seq, we identified 6,069, 5,785 and 5,575 potential target transcripts of QKI5, QKI6, and QKI7, respectively, in HepG2 cells. Among them, 3,312 transcripts were shared by all three QKIs (Figure S2I and S2J). When integrating QKI RIP-seq data with m^7G MeRIP-seq data, approximately 30% of internal m^7G-modified transcripts overlapped with putative targets of QKI5, QKI6, and QKI7 (Figure 2M). We incorporated our in-house QKI RIP-seq data with a single-site resolution (antibody-free) mapping of internal m^7G[18] and

observed a similar ~30% overlap between internal m^{7}G-modified transcripts and potential QKI targets (Figure S2K). We also integrated our QKI RIP-seq data with m^{7}G MeRIP-seq from *METTL1*-depleted HepG2 and observed a similar overlapping percentage between QKI-bound transcripts and m^{7}G-modified transcripts whose internal m^{7}G levels were decreased by *METTL1* depletion (Figure S2L).

The classic RNA recognition elements (RREs) of QKIs were “ACUAAY” or “YUAAY” (Y = C/U).[35,36] Consistently, the top motif of QKI5, QKI6 and QKI7 in our RIP-seq was UUAAUA (QKI5) or ACUAAC (QKI6 and QKI7) (Figure 2N). Intriguingly, the second most enriched QKI motif “GANGA (N = A/C/U/G)” is highly analogous to our internal m^{7}G motif “GANGAN” (Figure 2N). Particularly, the QKI7 “GANGAN” motif is identical to internal m^{7}G motif (Figures 2L *vs.* 2N). More importantly, the distribution of m^{7}G peaks and QKI-binding peaks was found to overlap very well at the whole transcriptome level (Figure 2O). Such data indicate that besides the conserved classic RREs, QKIs also recognize internal m^{7}G motifs in mRNAs.

To further corroborate the dependence of METTL1-mediated internal m^{7}G for the binding ability of QKI with target mRNAs, we analyzed m^{7}G MeRIP-seq and QKI7 RIP-seq from *METTL1*-depleted HepG2 cells. *METTL1* depletion led to a significant decrease of 3,254 m^{7}G peaks, while a significant increase of merely 1,002 peaks, suggesting that METTL1 had a global effect on mRNA internal m^{7}G modification (Figure S2M). METTL1 depletion-mediated increase of 1,002 m^{7}G peaks might be attributed to unappreciated indirect effects. Similar changes have been observed in m^{6}A-modified mRNAs: depletion of m^{6}A methyltransferases, METTL3 and METTL14, reduces global m^{6}A level but also results in an unexpected increase of m^{6}A peaks in many mRNAs in various cells.[37–39] Intriguingly, *METTL1* depletion globally suppressed QKI7-binding peaks, with hypo-binding peaks (4,723) double the number of hyper peaks (2,167) (Figures 2P and 2Q). Additionally, *METTL1* KO selectively attenuated QKI’s binding to “GANGAN” motif-containing targets (Figure S2N), suggesting that METTL1 is indeed responsible for QKI7’s binding to m^{7}G-modified transcripts. Finally, we performed KEGG analysis with m^{7}G-modified & QKI-bound transcripts to evaluate their biological functions and found that they are enriched in the “Endocytosis”, “pathways in cancer”, “Hippo signaling pathway” and “adherens junction” pathways (Figure S2O). Collectively, our results demonstrate METTL1 is responsible for mRNA internal m^{7}G methylation and QKIs specially recognize internal mRNA m^{7}G modification *in vitro* and *ex vivo*.

QKI6 and QKI7 bind to G3BP1 under stress conditions

QKI proteins contain three major domains, QUA1, KH, and QUA2 domains (Figure S3A), with QUA1 critical for homodimerization, and KH and QUA2 responsible for RNA binding.[36] Our data suggest the requirement of all three domains for internal m^{7}G recognition (Figure S3B). Despite only ~30 amino acids difference in the C-terminus (Figure S3A), the cellular localization of QKI5, QKI6, and QKI7 differs substantially. QKI5 is predominantly in the nucleus, while QKI6 and QKI7 are in both the nucleus and especially the cytosol (Figures 3A–3C and S3C).

Recent study revealed that mRNA internal m^7G is dynamically regulated and likely a key regulator of mRNA translation under stress conditions,[17] but the underlying mechanism is unknown. Stress adaption is essential for cell survival. Many stress conditions inhibit global mRNA translation and induce SG formation.[40] To investigate whether QKI interacts with core SG proteins and regulates fates of internal m^7G-modified mRNAs, we analyzed a protein-protein interaction database, GeneMANIA.[41,42] We found QKI closely interacts with multiple core SG proteins, including G3BP1, PTBP1, HNRNPK, etc. (Figure 3D). G3BP1 functions as a molecular switch to trigger liquid-liquid phase separation (LLPS) and SG assembly.[43] Therefore, we tested whether there is a direct interaction between G3BP1 and QKI6/QKI7, which are predominantly located in the cytoplasm. Our Co-IP assays in U2OS and HeLa cells, which have been extensively used for RNA granule studies,[22,43–45] revealed that QKI6 bound to G3BP1 under normal and stress conditions, while QKI7 interacted with G3BP1 only under stress conditions (Figures 3E and 3F). Furthermore, our *in situ* proximity ligation assay (PLA) confirmed the physical interaction between QKI6/QKI7 and G3BP1 within SGs (Figures 3G and 3H). Immunofluorescence (IF) staining reaffirmed that QKI6/7 mostly colocalized with G3BP1 in the cytosolic SGs, while QKI5 was restricted in the nucleus (Figures 3I–3K, and S3D). QKI6-RFP and QKI7-RFP fusion proteins also clearly colocalized with G3BP1-GFP in SGs (Figures 3L and S3E–S3H). We further constructed 6 truncated QKI proteins and found that the C-terminus, especially the D2 fragment (amino acids 268–312) is essential for the interaction with G3BP1 (Figures 3M, S3I, and S3J). The interaction between QKI6/7 and G3BP1 is RNA-independent (Figures S3K–S3M). Similarly, we found the N-terminal nuclear transport factor-like 2 (NTF2) domain of G3BP1 is required for its interaction with QKI (Figures S3N–S3P).

Taken together, our data indicates that QKI6 and QKI7 directly interact with SG core protein G3BP1 and colocalize within SGs under stress conditions, implying that QKI may play a role in mRNA metabolism during stress.

QKI7 shuttles internal m^7G-modified mRNA into SGs under stress

Recent studies suggest that RNA modifications might fine-tune the recruitment of certain RBPs and mRNAs into SGs, affecting cellular responses to stress.[22–24] To explore whether QKI shuttles internal m^7G-modified mRNAs into SG and modulates their fates, we imaged polyA signals and internal m^7G signals simultaneously in HeLa and U2OS cells under stress conditions (Figure 4A). While under normal conditions, both signals appeared diffused throughout the cytoplasm, we observed their accumulation in SGs under stress (Figures 4B and S4A). Quantitative analysis indicated that internal m^7G was more enriched in SGs under stress than polyA signal (Figures 4C and S4B), demonstrating that internal m^7G-modified mRNAs are preferentially recruited into SGs. We further validated this by evaluating the internal m^7G levels in the cap-depleted mRNAs from insoluble RNA granules (RGs), cytosol, and nucleus, and found RG mRNAs had higher internal m^7G levels, especially under stress (Figure 4D). *METTL1* KO significantly mitigated internal m^7G signal in SGs, and overexpression of wild-type METTL1, but not catalytically inactive METTL1, restored the m^7G signal (Figures 4E–4G), indicating the requirement of METTL1 methyltransferase activity for enriching internal m^7G-modified mRNAs in SGs.

To understand how stress induces the accumulation of m^7G-modified mRNAs in SGs, we first checked the expression levels of m^7G-binding proteins, m^7G methyltransferase, and core SG protein (G3BP1), but did not find any significant increase in their expression upon heat shock or sodium arsenite treatment (Figures S4C–S4E). Additionally, we observed no significant increase in internal m^7G abundance in global cap-depleted mRNAs under stress (Figure S4F). Furthermore, depletion or overexpression of *QKIs* did not significantly alter the internal m^7G level of cap-depleted mRNAs (Figures S4G–S4K) or the expression levels of METTL1 and G3BP1 (Figures 4H–4J). Based on current knowledge, mRNAs comprise over 70% of SG-enriched RNAs,[46] and the single-molecule mRNA tracking system strongly suggested that mRNAs shuttle in and out of SGs rapidly and dynamically.[47,48] Because stress substantially promotes the interaction of QKI7 with G3BP1 (Figures 3E and 3F), we speculated that QKI7 might bind to internal m^7G-modified mRNAs and shuttle them into SGs under stress conditions. Indeed, we found that the internal m^7G levels in SGs upon sodium arsenite treatment were significantly decreased by *QKI* depletion (Figures 4K, S4L, and S4M). Furthermore, *QKI* KO-mediated decrease of internal m^7G in SGs was partially restored by restoration of wild-type QKI7, but not truncated QKI that could not bind to internal m^7G (Figures 4L–4N). *QKI* KO significantly decreased the overall internal m^7G abundance in SG-enriched $polyA^+$ mRNAs, and the opposite was true when QKI7 was overexpressed (Figure 4O). Additionally, QKI7 is not a constitutive SG component as its depletion or overexpression did not influence SG numbers (Figures S4N–S4Q). Besides internal m^7G, m^6A-modified mRNAs are also more associated with SGs than unmethylated mRNAs.[22] Since m^6A is the most abundant mRNA modification and m^6A-binding YTHDF proteins recruit m^6A-modified mRNAs into SGs and promote phase separation and SG formation,[23,24] we investigated the relationship between m^7G and m^6A modifications in mRNAs. The m^7G RIP assay showed that m^6A levels in m^7G-IP mRNAs are higher than those in the input and significantly higher than the m^7G-depleted mRNAs (Figures S4R–S4T), and vice versa for m^7G levels in m^6A-IP mRNAs (Figure S4U), implying co-occurrence of m^7G and m^6A modifications in mRNAs. However, *METTL1* depletion does not affect expression of m^6A methyltransferases (and vice versa) or global m^6A abundance in mRNAs (Figures S4V and S4W), suggesting that internal m^7G and m^6A depositions are largely independent. Overall, our results suggest that QKI7 recognizes cytosolic internal m^7G-modified mRNAs and shuttles them into SGs under stress conditions.

Transcriptome-wide analysis of QKI7-bound and internal m^7G-modified mRNAs in SGs

Consistent with our findings in HepG2 and HeLa cells, QKI also had a stronger binding activity toward internal m^7G-modified mRNAs in U2OS cells, a canonical model cell line for SG study (Figure S5A). To comprehensively investigate the effects of QKI7 on the metabolism of SG-enriched mRNAs, we employed QKI7 RIP-seq and m^7G MeRIP-seq in U2OS cells. We showed that, in U2OS cells, QKI7 also had both the “GANGAN” internal m^7G motif (top one) and the “ACUAAC” canonical RRE motif (top two), and the internal m^7G modification notably enriched in the “GANGAN” context (top one) (Figure 5A). Most of the QKI7-bound peaks in U2OS cells were also enriched in mRNAs, rather than other RNA types (Figures S5B–S5E), and the internal m^7G decorations were also enriched around start codon (Figures S5F and S5G). Additionally, both QKI7-bound transcripts and internal m^7G-modified transcripts were quite conserved between different

cell types (Figure S5H). Moreover, 52.6% (1,233/2,342) of m^7G-modified transcripts were also identified as QKI7-bound transcripts in U2OS cells (Figure S5I). We further integrated our sequencing data with the widely used SG RNA-seq dataset from U2OS cells that identified 1,626 SG-enriched and 1,779 SG-depleted transcripts in U2OS cells.[19] Strikingly, 63.4% of the SG-enriched genes are QKI7-bound transcripts as detected by our RIP-seq, whereas merely 13.8% of the SG-depleted genes belong to QKI7-bound mRNAs (Figures 5C and 5D), supporting our notion that QKI7-bound transcripts are highly enriched in SGs. The percentage of the SG-enriched genes that belong to QKI7-bound and internal m^7G-modified transcripts is much higher than that of the SG-depleted genes (Figure 5E). Statistical analysis further confirmed the preferential localization of internal m^7G-modified mRNAs in SGs (Figure S5J).

Further pathway enrichment analysis showed that “Hippo signaling pathway” and “Pathways in cancer” are enriched with the “m^7G-modified & QKI7-bound genes” and “m^7G-modified & QKI7-bound & SG-enriched genes” in U2OS cells (Figures 5F and S5K), consistent with the analysis in HepG2 cells (see Figure S2O). Furthermore, 11 and 17 of the “m^7G-modified & QKI7-bound & SG-enriched transcripts” belong to the core-enriched genes in the “Hippo signaling pathway” and “Pathways in cancer”, respectively (Figure 5G). We then evaluated the abundance of those core-enriched genes in the insoluble SG-enriched fractions from U2OS cells upon *QKI7* overexpression or KO (Figures 5H and 5I). As expected, among the 28 core-enriched genes, 23 of them were significantly enriched in SGs when *QKI7* was overexpressed; while 16 of them were depleted in SGs when *QKI7* was depleted (Figure 5J). These 16 genes were therefore considered as the “SG-responsive genes”. Remarkably, overexpression of wild-type QKI7, but not truncated one, could fully rescue the *QKI* KO-mediated suppression of the enrichment of those mRNA targets in SGs (Figure S5L). Together, our studies reveal that QKI7 likely functions as a driver to orchestrate the recruitment of m^7G-modified transcripts into SGs and thereby modulates the cellular activities under stress conditions.

QKI7 regulates the stability and translation efficiency of a set of internal m^7G-modified mRNAs under stress conditions

Numerous studies have shown that following exposure to a stressful environment, RBPs can regulate a wide range of cytoplasmic processes, such as RNA stability, RNA storage, translation efficiency, and localization to cytoplasmic granules.[49,50] Since we have shown that internal m^7G-modified mRNAs are highly accumulated in SGs, we sought to assess whether QKI can regulate the fate of these m^7G-modified mRNAs in SGs. Via mRNA stability profiling, we showed that *QKI* KO significantly decreased the global mRNA half-life, while forced expression of wild-type QKI7, but not the truncated one, could largely rescue such phenotype (Figure 6A). These potential target genes overlapped well with QKI7-bound transcripts (Figure 6B) and SG-enriched transcripts (Figure 6C). Consistent with the previous SG enrichment data (Figures 5J and S5L), QKI could regulate the half-life of these representative SG-responsive genes (Figure 6D), implying that QKI7 overexpression may shuttle and store these genes into SGs and improve their stability under stress conditions. Our polysome profiling results indicated that neither *QKI7* overexpression nor depletion significantly influenced the overall translation efficiency (Figures S6A and

S6B). Nevertheless, when analyzing the distribution of QKI in different polysome fractions, we noticed that, under normal conditions, QKI7 was retained in free ribonucleoproteins; whereas under stress conditions, QKI7 shifted to 40S and 60S ribosomal subunit fractions (Figure 6E), where the condensing translation initiation complexes are formed[51,52]. Such data suggest that, although QKI7 showed mild effect on global protein synthesis, it might potentially regulate translation efficiency of a set of its target mRNAs, especially under stress conditions. Thus, we carried out RNA-seq as well as Ribo-seq to evaluate the effect of QKI7 on translation efficiency under stress conditions. We found that overexpression of QKI7 significantly attenuated the translation efficiency of both “QKI7-bound transcripts” and “SG-enriched transcripts” (Figures 6F and 6G).

To identify the translation-dependent direct mRNA targets of the QKI-m^{7}G-SG axis, we mainly focused on the candidates in the “Hippo signaling pathway” and/or “Pathways in cancer”, as these two pathways are the top enriched pathways for the SG-enriched m^{7}G-modified and QKI7-bound genes (see Figures 5F and 5G). Amongst the 16 validated “SG-responsive genes”, we identified 5 candidate target genes, including *GSK3B, TEAD1, ROCK1, IGF1R*, and *BMPR2*, with potentially decreased translation efficiency upon QKI7 overexpression (Figures 6H–6J). *QKI7* overexpression significantly reduced the enrichment of these candidate target mRNAs except for *BMPR2* in polysome fractions under stress conditions (Figures 6H–6I and S6C), supporting the notion that QKI7 sequesters its mRNA targets within SGs and suppresses their translation under stress. Next, ourm^{7}G-MeRIP qPCR verified the internal m^{7}G sites of *GSK3B*, *TEAD1*, *ROCK1* and *IGF1R* mRNAs (Figure S6D). METTL1 and WDR4 are highly enriched on these transcripts (Figures S6E and S6F) and *METTL1* depletion caused a significant decrease of internal m^{7}G abundance in these transcripts (Figure S6G), confirming that the METTL1-WDR4 complex is responsible for adding internal m^{7}G into these transcripts. Moreover, *METTL1* depletion significantly suppressed the binding of QKI7 with these transcripts (Figure 6K). We further showed that QKI7 overexpression markedly decreased the protein level and translation efficiency of GSK3B, TEAD1, ROCK1 and IGF1R, but not their mRNA levels, following sodium arsenite treatment (Figures 6L and S6H–S6J). Finally, we optimized the $NaBH_4$ and KBH_4-mediated reduction plus aniline-promoted RNA cleavage assays to authenticate the existence of m^{7}G at internal sites. The single m$^7G_{1639}$ site in 18S rRNA was included as a positive control. Our Northern blot and qPCR showed that reduced 18S rRNA could be specifically and efficiently cleaved by aniline into two fragments (Figures S6K–S6N). We followed this strategy to verify the internal m^{7}G sites in *IGF1R* mRNA transcript (as a representative). Both a specific m^{7}G site (m^{7}G11056)[18] and an m^{7}G peak (revealed by our m^{7}G MeRIP-seq) in *IGF1R* were included (Figure S6O). Aniline treatment did induce the cleavage of the reduced *IGF1R* in both regions (Figure S6P), while *METTL1* KO largely blocked aniline-mediated cleavage (Figure S6Q), verifying the existence of internal m^{7}G modifications in *IGF1R* mRNA. Overall, our results suggest that the internal m^{7}G binding protein QKI7 fine-tunes the stability and/or translation efficiency of a set of m^{7}G-modified transcripts under stress by sequestering them in SGs (Figure 6M).

QKI7 sensitizes cancer cells to chemotherapy drugs

In tumor microenvironment, cancer cells are exposed to adverse and stressful conditions, including hypoxia, hypoglycemia, inflammation, and chemical poisoning, which can trigger the assembly of SGs.[53] Recently, accumulating evidence has linked the formation of SGs to chemotherapeutic treatment and cancer cell survival.[54] Our analysis of the TCGA dataset revealed a significant positive correlation between *QKI* and SG core components in expression across various cancer types (Figure 7A), implying that QKI may play a broad role in SG-related bioprocesses in cancer. To explore the clinical relevance of our findings, we sought to investigate whether QKI and internal mRNA m^7G modification are involved in SG-related chemotherapy resistance. Here, we utilized doxorubicin treatment as a representative chemotherapeutic stress and showed that it could trigger SG assembly in cancer cells and QKIs were localized within the doxorubicin-driven SGs (Figures S7A–S7C). Notably, overexpression of QKIs significantly decreased the IC_{50} values of doxorubicin in parental cancer cells, but not in *METTL1* KO cells (Figures 7B and 7C), indicating that METTL1 is required for QKI-induced sensitization of cancer cells to doxorubicin. Overexpression of *QKI*s cannot significantly affect cancer cell proliferation (Figure 7D), suggesting QKIs-mediated response to chemotherapy was not associated with changes of cell proliferation. Instead, QKI7 overexpression and depletion significantly promoted and inhibited doxorubicin-induced apoptosis, respectively, in cancer cells (Figures 7E and 7F). Clonogenic survival assays also showed that QKI7 overexpression and KO conferred and inhibited the sensitivity of cancer cells to doxorubicin, respectively (Figure 7G). *G3BP1* KO largely mitigated the effect of QKI7 overexpression on sensitizing cancer cells to doxorubicin treatment, suggesting that such function of QKI7 is dependent on SG formation (Figure S7D–S7E). Our *in vivo* xenograft model verified that *QKI7* overexpression did not impact tumor proliferation, but significantly enhanced the sensitivity of the tumors to doxorubicin treatment (Figures 7H–7J). The Hippo signaling pathway has emerged as a linchpin in drug resistance in various tumors and GSK3B is a pivotal mediator of chemotherapy resistance.[55–57] Under doxorubicin-induced stress conditions, QKI7 overexpression remarkably decreased the protein levels of GSK3B and TEAD1 (Figure S7F), two core enriched genes in the Hippo signaling (Figure 6J); moreover, *GSK3B* and *TEAD1* overexpression could partially reverse QKI7-induced drug sensitivity (Figures S7G and S7H), indicating that the QKI7-m^7G axis-mediated silencing of the Hippo signaling pathway might contribute to the elevated sensitivity of cancer cells to chemotherapy.

Analysis of the liver cancer pharmacogenomic landscape study dataset[58] also revealed that the liver cancer cell lines with QKI7 high expression (HepG2 and Hep3B) are much more sensitive to various chemotherapy or targeted therapeutic drugs compared to those with QKI7 low expression (MHCC97H and SNU475) (Figures 7K–7M and S7I–S7J). We confirmed that HepG2 and Hep3B cells showed lower IC_{50} values of doxorubicin as well as sorafenib (Figures S7K and S7L). Collectively, our results indicate that the mRNA internal m^7G modification binding protein QKI7 sensitizes various cancer cells to chemotherapy drugs (e.g., doxorubicin and sorafenib).

Discussion

Our data and those from others[17,18] indicate that m^7G is not restricted to the 5' cap of mRNAs but also occurs internally in mRNAs. The internal m^7G/G level ranges from 0.01% – 0.03% in the mRNAs from different cell lines, and the METTL1-WDR4 complex is responsible for adding m^7G into internal mRNA regions. We characterized the transcriptome-wide profile of internal m^7G modification, revealed its enrichment near the start codons, and unveiled the highly conserved internal m^7G motif, GANGAN. More strikingly, under stress conditions, the mRNAs with internal m^7G modification are enriched in the SGs, suggesting the internal m^7G decoration might respond to certain physiological conditions.

Here we report that QKI proteins (QKIs) selectively bind to internal m^7G modification in mRNAs. Notably, approximately 30%−50% of the mRNA transcripts with internal m^7G could be directly recognized by QKIs. The QKIs have both m^7G-dependent targets (with "GA-rich" motifs) and m^7G-independent targets (with the "ACUAAC" motif). Moreover, the integrative analysis of QKI RIP-seq and m^7G MeRIP-seq data revealed that QKI-binding sites and m^7G peaks are well correlated and overlapped in mRNA transcripts.

Among the three major isoforms of QKIs, QKI5 is predominantly located in the nucleus, but QKI6 and QKI7 are distributed in both nucleus and especially cytoplasm. As internal m^7G-modified mRNAs are mainly located in cytoplasm, QKI6 and QKI7, rather than QKI5, are likely the major m^7G-binding proteins. During stress, RNAs and RBPs form the membraneless SGs in the cytoplasm to support cell survival. Interestingly, we found that stress conditions facilitate the enrichment of m^7G-modified mRNAs into SGs. Coincident with this, stress conditions also promote the direct interaction of QKI7 with G3BP1, while QKI6 shows a similar degree of interaction with G3BP1 under normal and stress conditions, suggesting that QKI7 may play a major role in shuttling internal m^7G-modified mRNAs into SGs under stress. Indeed, our further studies suggest that QKI7 recognizes and shuttles hundreds of internal m^7G-modified mRNAs into SGs. Moreover, *METTL1* depletion not only attenuates the internal m^7G-modified mRNA enrichment in the SGs, but also impairs the global binding of QKI7 with its internal m^7G-modified targets.

Although the connection between SG assembly and mRNA metabolism has been extensively studied, the causality between SG formation and translation inhibition is controversial. Previous studies have suggested that SG assembly may act as a driver to induce translation inhibition under stress conditions.[59,60] Nevertheless, other studies argued that SG formation might be a consequence of translation inhibition because the cells without endogenous G3BP1/2 expression still undergo translation repression.[51] Given that merely 10% of bulk mRNA molecules are present in SGs,[19] it is possible that SG formation regulates the translation efficiency of a set of specific transcripts, and does not significantly influence protein synthesis globally. In our study, we have shown that although *QKI* depletion does not affect global mRNA translation efficiency, *QKI* KO does attenuate the translation of a subset of downstream targets. In addition, *QKI* depletion leads to a global decrease in mRNA half-life and such effect largely relies on its ability to recognize internal m^7G modification. We propose that QKIs, especially QKI7, not only recruit hundreds of internal

m^{7}G-modified mRNAs into SGs and protect them to be degraded, but also abrogate translation of a subgroup of target mRNAs to adapt to the stress conditions. Our validation assays confirmed that QKI7 suppresses translation efficiency of several representative “SG-responsive” mRNA targets carrying internal m^{7}G, including the core-enriched genes in the “Hippo signaling pathway” (e.g., *GSK3B* and *TEAD1*) and in the “pathways in cancer” (e.g., *ROCK1* and *IGF1R*), under stress conditions. It would be interesting and necessary to investigate how QKI and internal m^{7}G modification determine the fate of other target mRNAs in the future.

The diverse genomic and epigenomic landscapes of cancer cells play an essential role in multiple therapeutic resistance, which remains the primary hindrance to curative cancer treatment.[61] More recently, evidence is emerging that the formation of SGs is extensively involved in therapeutic resistance and SGs may act as an indicator of chemoresistance.[62,63] We showed here that doxorubicin, a first-line chemotherapy drug, induces the assembly of SGs in cancer cells and enhances interaction of QKI7 with G3BP1. Ectopic expression of QKI7 sensitizes cancer cells to doxorubicin treatment *in vitro* and *in vivo*, associated with suppression of translation of a set of targets including the core genes in the Hippo signaling pathway (e.g., *GSK3B* and *TEAD1*). Moreover, analysis of the TCGA database also showed a significant positive correlation between *QKI* and SG markers, indicating a possible connection between m^{7}G binding protein QKI and SGs in various types of cancers. Thus, QKIs may play a broad role as mRNA internal m^{7}G binding proteins in regulating cancer cells’ stress environment response and drug resistance. Further investigations are required to obtain a deeper understanding of the role of QKI, internal m^{7}G modification and SG formation in various cancer types towards different therapeutic drugs.

In summary, our findings reveal a previously unappreciated role of QKIs as mRNA internal m^{7}G binding proteins, provide profound insights into the biological function of QKIs and internal m^{7}G modification in rewiring the SG transcriptome under stress conditions, and highlight the therapeutic potential of targeting QKIs (especially QKI7) to reinforce chemotherapy for curative treatment.

Limitations of the study

In eukaryotic mRNAs, m^{7}G modification is frequently located at the 5’ cap regions and current m^{7}G antibodies fail to distinguish between m^{7}G cap and internal m^{7}G sites, which may lead to unwanted contamination. In the present study, the first 100 nucleotides of the 5’ were trimmed during m^{7}G MeRIP-seq analysis to minimize m^{7}G cap contamination. The abundance of internal m^{7}G modifications is relatively low, which warrants the development of more sensitive and accurate methods to precisely detect it. At current stage, it is still unknown which enzyme(s) serves as the demethylase(s) of internal mRNA m^{7}G modification and how its methyltransferases and demethylase(s) dynamically fine-tune internal m^{7}G abundance across the transcriptome. Identification of all the major methyltransferases, demethylase(s) and binding proteins of internal mRNA m^{7}G will facilitate our systematical studies of the biological functions of internal mRNA m^{7}G in normal bioprocesses and disease development. Additionally, although we have demonstrated that QKI7 shuttles internal m^{7}G-modified transcripts into SGs, the underlying mechanism

regarding how QKI7 interacts with G3BP1 and responses under stress conditions has yet to be fully characterized. Moreover, as a type of classic RBPs, QKIs play critical roles in regulating RNA alternative splicing, microRNA processing, nuclear export, and circRNA biogenesis.[26,64–66] Therefore, it would be interesting to investigate whether such functions of QKIs rely on their ability to recognize mRNA internal m^7G modification.

STAR Methods

RESOURCE AVAILABILITY

Lead Contact—Further information and requests for resources and reagents may be directed to and will be fulfilled by the Lead Contact, Jianjun Chen (jianchen@coh.org).

Materials Availability—All cell lines, plasmids, and other stable reagents generated in this manuscript are available from the Lead Contact under a complete Materials Transfer Agreement.

Data and Code Availability

- All sequencing data generated in this study have been deposited at GEO and are publicly accessible under accession numbers GSE193039, GSE218221, and GSE218222. The binding motifs of METTL1, IGF2BP1, LRPPRC and QKI were identified by ENCORI (https://rna.sysu.edu.cn/). The potential protein-protein interaction for QKI was predicted from GeneMANIA (http://genemania.org/). The raw data for correlation analysis between *QKI* and *EIF2A*, *G3BP1*, *G3BP2*, *PABPC1*, *TIA1* and *TIAL1* were derived from TCGA (http://cancergenome.nih.gov/).
- This paper does not report original code.
- Any additional information required to reanalyze the data reported in this work paper is available from the Lead Contact upon request.

EXPERIMENT MODEL AND SUBJECT DETAILS

Cell Culture—The human HepG2, HeLa, HEK293T, U2OS, THLE-2, SNU475, Hep3B, and SNU449 cell lines were obtained from American Type Culture Collection (ATCC). The Huh7 and MHCC97H cell lines were kindly provided by Dr. Wendong Huang (City of Hope, Duarte, CA). All these cell lines were cultured in DMEM medium (Thermo Fisher Scientific) supplemented with 10% fetal bovine serum (Gemini Bio-Products) and 1% penicillin/streptomycin (Thermo Fisher Scientific) at 37°C in a 5% CO_2 humidified incubator. All the cell lines were identified by STR cell authentication and routinely tested for mycoplasma contamination using PCR Mycoplasma Detection Kit (G238, Applied Biological Materials). The culture medium was changed 24h before stress conditions. Arsenite stress was induced by treating with 500 μM sodium arsenite (1062771000, Millipore) for 0.5–2h as indicated. For heat shock experiments, cells were incubated at 42 °C for 1h.

Animal Studies—The immunodeficient NOD.Cg-*Prkdc*^{scid} *Il2rg*^{tm1Wjl}/SzJ (NSG) mice were purchased from Jackson Laboratory (Jax_005557) and bred at the specific-pathogen-free core facilities of City of Hope. All the mice were housed on a 12h-12h light-dark cycle. The HeLa cells were infected with empty vector or QKI7 overexpression virus and selected with 2 μg/ml puromycin (ant-pr-1, InvivoGen) for five days before animal studies. To construct the tumor-bearing mouse model, the stable HeLa cell lines (1×10^7) were injected subcutaneously into 6-week-old male NSG mice. When tumor volumes reached 100 mm^3, the NSG mice were randomly allocated into two sub-groups (n=7) and then doxorubicin (44583, Sigma-Aldrich) treatment was started. Doxorubicin was administered through intraperitoneal (i.p.) injection at 1 mg/kg every three days, for a total of four times. For control group, the same volume of vehicle was intraperitoneally injected. Tumors were measured using a caliper and the tumor volume was calculated as (length × width^2/2). Mice were euthanized when they met the institutional euthanasia criteria for tumor size. At the end-point, tumors were collected and weighted. All the animal experiments were compliant with federal and state government guidelines and the Institutional Animal Care and Use Committee (IACUC) protocol approved by City of Hope.

METHOD DETAILS

Plasmid Construction—Human METTL1, WDR4, QKI5, QKI6, QKI7, GSK3B and TEAD1 genes were amplified by CloneAmp HiFi PCR Premix (639298, Takara) using human cDNA made from HEK293T cell and then subsequently cloned into lentivector-based pMIRNA1 (SBI) or pCDH (46970, Addgene) vectors. Catalytically inactive METTL1, synonymous mutated METTL1, synonymous mutated QKIs, truncated QKIs (ΔC, ΔQUA1, ΔKH, ΔQUA2, ΔQD1 and ΔD2), and truncated G3BP1s (ΔNTF2, ΔRRM and ΔRGG) were constructed by In-Fusion cloning Plus CE (638916, Takara) according to the manufacturer's instruction. *QKI* shRNAs were purchased from Sigma-Aldrich (SHCLNG-NM_006775). All the primers used for molecular cloning were listed in Table S1. The plasmids were extracted using QIAprep Spin Miniprep Kit (27104, Qiagen) and validated by Sanger sequencing (Eton Bioscience).

Lentivirus Production and CRISPR/Cas9-Based Knockout—The sgRNAs against *METTL1*, *WDR4*, *QKI* and G3BP1 were designed using CRISPick (https://portals.broadinstitute.org/gppx/crispick/public) and then cloned into lentiGuide-hygro plasmid (104991, Addgene) via DNA Ligation Kit (6023, Takara). The scramble sgRNA sequence (5′-TGCGAATACGCCCACGCGATGGG-3′) was designed to target the LacZ gene from *Escherichia coli*. To generate the lentiviruses for knockout of those genes, the 2nd generation lentiviral packaging vectors (2.25 μg psPAX2 and 0.75 μg pMD2.G), 3 μg lentiCas9-Blast plasmid (52962, Addgene), or 3 μg lentiGuide-hygro sgRNA were co-transfected into HEK293T cells using X-tremeGENE™ HP DNA Transfection Reagent (6366546001, Sigma-Aldrich) in 6-cm dishes. The media with lentiviruses were harvested at 48 h and 72 h post-transfection and filtered using 0.45μm syringe filter. Then, the Cas9-expressing lentivirus particles were added into HepG2, HeLa, and U2OS cells directly with 8 μg/ml polybrene (H9268, Sigma-Aldrich). After two rounds of infection, the Cas9 single clones of HepG2, HeLa, and U2OS were selected with 20 μg/ml blasticidin (ant-bl-1, InvivoGen) and allowed to grow for 3–4 weeks. The single clones were infected with

sgRNA-expressing lentivirus and selected with hygromycin (ant-hg-5, InvivoGen, 100 μg/ml for U2OS, 200 μg/ml for HeLa; 500 μg/ml for HepG2). The sequences of these sgRNAs were listed in Table S1, knockout efficiencies were validated by Western blotting.

Cell Proliferation Assay—The HeLa and U2OS cells were infected with indicated lentivirus and selected for 1 week to generate stable knockout or overexpression cells. The cells were seeded into 96-well plates at a density of 4×10^3 cells per well in a final volume of 100 μl. Cell proliferation was determined by Cell Counting Kit 8 (CK04, Dojindo) and measured at OD 450 nm using BioTek Gen5 system (BioTeck, USA) according to the manufacturer's instruction.

Clonogenic Survival Assays—The cells were seeded at 5×10^3 cells per well in 6-well plates and cultured in medium containing doxorubicin with indicated concentration. Fresh medium with doxorubicin was changed twice a week. After 14 days, the emerging colonies were washed gently with PBS, fixed with 4% formaldehyde and then stained with 0.1% (w/v) crystal violet for 15 min. The relative growth was measured by dissolving cell-bound crystal violet in 2ml 10% (v/v) acetic acid. The absorbance of dissolving crystal violet was measured at 595 nm using BioTek Gen5 system (BioTeck, USA).

Flow Cytometry Analysis of Apoptosis—Stable HeLa and U2OS cells were seeded into 6-well plates at a density of 5×10^5 cells per well 48 hours before the apoptosis assay. Then cells were then treated with DMSO or doxorubicin for 24 hours. After drug treatment, cells were harvested by trypsinization, washed twice with PBS, stained with APC Annexin V Apoptosis Detection Kit (640932, Biolegend) following the manufacturer's instructions. Flow cytometry was performed using Fortessa X20 (BD Biosciences, USA) and the results were analyzed with FlowJo software.

Proximity Ligation Assay (PLA)—The PLA assay was carried out as reported previously.[67] Briefly, the cells were transfected with FLAG-tagged QKI5, QKI6 or QKI7 48 hours before the PLA assay. Then 1×10^4 cells were seeded on an 8-well chamber slide (154534, Thermo Fisher Scientific). 500 μM $NaAsO_2$ was added in the chamber for 1 h to induce the forming of stress granules (SGs). Then wash the cells three times with PBS, followed by fixed with 4% paraformaldehyde for 15 min at room temperature. The cells were then incubated with 1 × Permeabilization Buffer (00-8333-56, Thermo Fisher Scientific) for 15 min and rinsed by PBS three times. Subsequently, the cells were blocked with Duolink block solution for 1 hour at room temperature and incubated overnight at 4°C with the following antibodies: mouse anti-FLAG antibody (1:500, F3165, Sigma-Aldrich) & rabbit anti-G3BP1 antibody (1:300, 13057-2-AP, Proteintech). Empty Vector transfected U2OS cells were used as negative control. The next day, the cells were washed with large volume of PBS two times and incubated in PLA probes (DUO92002 and DUO92004, Sigma-Aldrich) for 1 h at 37 °C. Afterward, the cells were washed with 1× Duolink *In Situ* Wash Buffer A (DUO82049, Sigma-Aldrich) twice for 5 min and incubated with ligation mix at 37 °C for 30 min. After that, the cells were washed with 1× Duolink *In Situ* Wash Buffer A twice and incubated with amplification mix (DUO92008, Sigma-Aldrich) at 37 °C for 100 min. In the end, the cells were washed twice with 1× Duolink *In Situ* Wash

Buffer B, washed once with 0.01× Buffer B, and mounted with Duolink *In Situ* Mounting Medium with DAPI (DUO82040, Sigma-Aldrich). The pictures were captured under LSM 880 confocal microscope with Airyscan model (Zeiss, Germany).

Simultaneous polyA FISH and m^{7}G Immunofluorescence Staining—The PolyA FISH and immunofluorescence staining was performed by referring to the published literature[22] with some modifications. Here, we used methanol fixation to remain large RNAs but not small RNAs such as microRNA, tRNA and snRNA. We also included an additional step to refold rRNA which prevents the binding between rRNA m^{7}G modification and m^{7}G antibody. The *in situ* mRNA decapping procedure was conducted using Tobacco Decapping Plus 2 (94, Enzymax). Thus, our m^{7}G-immunostaining protocol primarily detects mRNAs with internal m^{7}G modification.

Briefly, 1×10^4 cells were seeded on 8-well chamber slides 24 h before staining. The cells were washed once with pre-cold PBS and then fixed and permeabilized with 1 ml methanol at −20 °C for 10 min. After withdrawing the methanol, 70% ethanol was added into each well and incubated for 10 min to rehydrate the cells. Then cells were dried under air and equilibrated using Stellaris RNA FISH wash buffer A (SMF-WA1-60, LGC Biosearch Technologies) containing 10% formamide for 5 minutes. For *in situ* mRNA decapping, each chamber was incubated with 100 μl decapping reaction (10 μl 10× decapping reaction Buffer, 2 μl 50 mM $MnCl_2$, 2 μl Tobacco Decapping Plus 2 enzyme, and 86 μl 0.1% Triton X-100) at 37 °C for 2 h. Then the cells were washed three times with Stellaris RNA FISH wash buffer A. Cy5-polydT-LNA probe (sequence: /Cy5/ T+TT+TT+TT+TT+TT+TT+TT form IDT) was diluted in Stellaris RNA FISH hybridization buffer (SMF-HB1-10, LGC Biosearch Technologies) containing 10% formamide for a final concentration of 1 μM. The slides were then covered with RNA FISH hybridization buffer and incubated in a humidified 37 °C incubator overnight. The next day, slides were washed twice using Stellaris RNA FISH wash buffer A containing 10% formamide for 30 min each at 37 °C. The RNA FISH Wash buffer was stored at 4 °C and added directly to the slides before incubation at 37 °C, which helped to eliminate the staining of rRNA. Slides were then washed and equilibrated three times with PBS at room temperature for 5 min each, and blocked using blocking solution (2% BSA, 0.1% Triton-X100 in PBS) for 1 h at room temperature. The cells were subsequently incubated with anti-m^{7}G antibody (1:300, RN017M, MBL International) for 2 h at room temperature protected from light. After washing with PBS three times, Goat anti-Mouse secondary antibody was applied to the slides and kept incubating for 1 h at room temperature. The nuclei were stained by mounting the cells in Mounting Medium with DAPI (DUO82040, Sigma-Aldrich). The pictures were captured under LSM 880 confocal microscope (Zeiss, Germany).

Immunofluorescence Staining—1×10^4 cells were seeded on 8-well chamber slides 24 h before staining. After treatment with 500 μM $NaAsO_2$ for 1 h, the cells were washed with PBS three times and then fixed in 4% paraformaldehyde for 15 min at room temperature. The cells were then incubated with 1 × Permeabilization Buffer (00-8333-56, Thermo Fisher Scientific) for 15 min and rinsed by PBS three times. After that, cells were blocked in blocking solution (5% BSA with PBS) for 1 h at room temperature and incubated overnight

at 4 °C with the following primary antibodies (diluted in 1% BSA with PBS): mouse anti-FLAG antibody (1:500, F3165, Sigma-Aldrich) and rabbit anti-G3BP1 antibody (1:300, 13057-2-AP, Proteintech). On the second day, the cells were washed with PBS three times (10 min/each) and incubated with secondary antibodies plus Phalloidin (CF555 Conjugated) for 1 h at room temperature. After washed three times with PBS (10 min/each), the slides were mounted with *In Situ* Mounting Medium with DAPI (DUO82040, Sigma-Aldrich). The pictures were captured under Zeiss LSM 880 confocal microscope with Airyscan model (Zeiss, Germany) and analyzed by ImageJ. The colocalization was quantified by Colocalization Finder (Image J plug-in).

Western Blotting—The Western blotting was conducted as described previously.[68,69] The cells were lysed using RIPA Lysis and Extraction Buffer (R0278, Sigma-Aldrich) supplemented with 1% protease inhibitor cocktail (78438, Thermo Fisher Scientific) and phosphatase inhibitor cocktail (78426, Thermo Fisher Scientific). The cytoplasmic and nuclear protein fractions were separated using NE-PER™ Nuclear and Cytoplasmic Extraction Reagents (78833, Thermo Fisher Scientific) according to the manufacturer's instructions. Mitochondrial protein fraction was isolated using Mitochondria Isolation Kit (89874, Thermo Fisher Scientific). For Western blotting, equal amounts of proteins were separated by 10% SDS-PAGE gel and then transferred onto polyvinylidene difluoride (PVDF) membranes. Chemiluminescence signaling was detected by Pierce ECL Western Blotting Substrate (PI32106, Thermo Fisher Scientific) or Amersham™ ECL™ Prime Western Blotting Detection Reagent (RPN2232, Cytiva). Antibodies used for Western blotting were listed as follow: METTL1 (14994-1-AP, Proteintech), WDR4 (sc-100894, Santa Cruz), pan-QKI (13169-1-AP, Proteintech), QKI5 (A300-183A, Bethyl Laboratories), QKI6 (AB9906, EMD Millipore), QKI7 (75-200, NeuroMab), G3BP1 (13057-2-AP, Proteintech), LRPPRC (21175-1-AP, Proteintech), IGF2BP1 (8482S, Cell Signaling Technology), IGF2BP2 (14672S, Cell Signaling Technology), IGF2BP3 (A303-426A, Bethyl Laboratories), METTL3 (ab195352, Abcam), METTL14 (HPA038002, Sigma-Aldrich), IDH1 (8137S, Cell Signaling Technology), FLAG (F3165, Sigma-Aldrich), RPL7 (14583-1-AP, Proteintech), GSK3B (22104-1-AP, Proteintech), TEAD1 (13283-1-AP, Proteintech), ROCK1 (21850-1-AP, Proteintech), IGF1R (20254-1-AP, Proteintech), VDAC (10866-1-AP, Proteintech), and Histone H3 (4499S, Cell Signaling Technology). β-actin (3700S, Cell Signaling Technology), Vinculin (sc-73614, Santa Cruz), or GAPDH (10494-1-AP, Proteintech) were used as loading control.

Co-Immunoprecipitation (Co-IP)—1×10^7 HEK293T cells grown in 10-cm dishes infected with specific lentivirus were lysed within 500 μl Pierce™ IP Lysis Buffer (87787, Thermo Fisher Scientific) containing 1 × protease inhibitor cocktail (78438, Thermo Fisher Scientific) and 1 × phosphatase inhibitor cocktail (78426, Thermo Fisher Scientific) for 30 min on ice. The supernatant was then cleaned by centrifugation at 13,000 rpm for 15 min at 4 °C. For CO-IP with RNase digestion, 10 μl RNase A/T1 mix (EN0551, Thermo Scientific Scientific) was added to the protein lysates and incubated at room temperature for 30 min with gentle shaking. RNA was extracted from the lysates using QIAzol (79306, Qiagen) to validate the digestion effect before IP. One-tenth volume of protein lysate was kept as Input and the left part was mixed with 25 μl Protein A/G magnetic beads

(88803, Thermo Fisher Scientific) and rotated at 4°C for 1 h to reduce non-specific binding. Then, pre-cleared protein samples were incubated with mouse anti-FLAG antibody (F3165, Sigma-Aldrich), rabbit anti-G3BP1 antibody (13057-2-AP, Proteintech), normal mouse IgG (12–371, Millipore) or normal rabbit IgG (12–370, Millipore) under rotation overnight at 4°C. Then, 50 μl pre-cleaned Protein A/G magnetic beads (88803, Thermo Fisher Scientific) were added to the reaction and kept rotation for 4 h at 4°C. Proteins were washed three times with IP washing buffer (10 mM Tris-HCl pH 7.5, 1 mM EDTA, 1 mM EGTA, 150 mM NaCl, 1% Triton-X, 0.2 mM sodium orthovanadate) and then detected by Western blotting.

Electrophoretic Mobility Shift Assay (EMSA)—The EMSA was performed as previously described.[70] Briefly, fluorescein-labeled G-oligos and m^7G-oligos were denatured by heating at 65 °C for 5 min and slowly cooling down to room temperature. For each reaction, 1 μl RNA probes (5 nM final concentration) and 1 μl protein (0 nM, 40 nM, 80 nM, 120 nM, 160 nM, 200 nM final concentration) were incubated in 8 μl binding buffer (10 mM Tris-HCl pH 7.5, 50 mM KCl, 1 mM EDTA, 0.05% Triton X-100, 5% glycerol, 1 mM DTT and 40 U per ml RNasin) at 4°C for 30 min. The RNA–protein mixture was loaded to 6% TBE gel and run (in 0.5 × TBE buffer) on ice for 45 min at 90 V. The fluorescence signal was visualized by ChemiDoc MP imagine System (Bio-Rwad).

Reverse Transcription and Quantitative Real-Time PCR—The reverse transcription was performed with 0.2–1 μg total RNA and the QuantiTect Reverse Transcription Kit (205314, Qiagen) according to the manufacturer's instructions. The Quantitative real-time PCR (qRT-PCR) was conducted using SYBR Green qPCR Master Mix (FERK0253, Thermo Fisher Scientific) in the QuantStudio™ 7 Flex Real-Time PCR System to determine the mRNA expression level of a gene of interest. Gene expression levels were normalized to the expression of *GAPDH* or *ACTB*. All the primers used for qRT-PCR are listed in Table S1.

UHPLC-QQQ-MS/MS—To accurately evaluate the m^6A and internal m^7G levels in mRNAs, the $polyA^+$ RNAs were enriched from total RNA through two-round purification using oligo(dT) beads and the 5' Cap was removed from $polyA^+$ mRNAs with Tobacco Decapping Plus 2 (94, Enzymax). Then, 200 ng decapped mRNAs were digested in a two-step manner as previously described.[18] Firstly, 1 μl nuclease P1 (N8630, Sigma-Aldrich, dissolve to 1 U/μl in H2O) was added along with 2 μl 200 mM NH_4OAc (pH=5.3) in a 20 μl reaction and incubated at 42 °C for 2 h. Then add 2.1 μl 10× FastAP buffer and 1 μl FastAP Alkaline Phosphatase (EF0651, Thermo Fisher Scientific) to each reaction and incubate at 37 °C for 2 h. After digestion, the samples were diluted using LC-MS grade water to a 3 ng/μl final concentration and filtered with 0.22 mm filters (Millipore). 10μl of the entire solution was subjected to the LC-MS/MS for detection of m^7G, G, m^6A, and A. The UHPLC-QQQ-MS/MS was performed using an Agilent 6410 Triple Quadrupole Tandem Mass Spectrometer with an Agilent 1290 HPLC. Nucleosides were separated using a Kinetex C18 Reversed Phase column (30 × 2.1 mm, 1.7 μm, 100 Å). The amounts of nucleosides were calibrated by standards curves obtained from pure m^7G, G, m^6A, and A nucleoside standards (Cayman Chemical Company). The RNA m^7G level and m^6A level are calculated as the ratio of m^7G to G and m^6A to A, respectively.

m^{7}G and m^{6}A Dot Blot Assay—The mRNA m^{7}G and m^{6}A dot blot were conducted as previously described with minor modification.[17] The polyA$^+$ mRNAs were enriched from total RNAs with polyATract mRNA isolation system IV (Z5310, Promega) and the 5' Cap was removed from polyA$^+$ mRNAs with Tobacco Decapping Plus 2 (94, Enzymax). Then, the indicated amount of decapped polyA$^+$ mRNA was denatured in RNA incubation buffer (65.7% formamide, 7.77% formaldehyde and 1.33× MOPS) at 65 °C for 5 min, and then chilled on ice directly. An equal volume of 20 × SSC buffer was added to the samples and mixed thoroughly. The RNA samples were spotted on the Amersham Hybond-N$^+$ membrane (RPN303B, Cytiva) followed by UV-crosslink (254 nm UV for 5 min). Then the membrane was stained with 0.02% methylene blue in 0.3 M sodium acetate (pH 5.2). After capturing the image, the membrane was blocked with 5% non-fat milk in 1×PBST for 1 h, and incubated with anti-m^{7}G antibody (1:2000, RN017M, MBL International) or anti-m^{6}A antibody (1:5000, 202003, Synaptic Systems) overnight at 4 °C. On the next day, the membrane was washed for three times with 1×PBST and then incubated with HRP-conjugated anti-mouse secondary antibody (1:500) for 1h. The m^{7}G and m^{6}A signals were developed with Amersham™ ECL™ Prime Western Blotting Detection Reagent (RPN2232, Cytiva)

Detection of gene-specific internal m^{7}G sites by chemical-mediated cleavage —The $NaBH_4$ reduction and KBH_4 reduction of RNAs were performed by referring to previously established methods with optimization.[7,71] For $NaBH_4$ reduction method, 4 μg RNA in 15 μl 0.5 M Tris-HCl was either incubated as is (mock reaction) or mixed with 15 μl 1 M $NaBH_4$ in the presence of 3.75 mM m^{7}GTP (reduction reaction) and incubated on ice for 40 min. Another 15 μl 1M $NaBH_4$ was incubated with 60 μl 3 M sodium acetate (pH 5.5) and 240 μl nuclease-free water at 90 °C for 30 min and added to the mock reaction just before RNA precipitation by 30 μg glycogen and 990 μl of ice-cold absolute ethanol. The reduction reaction was precipitated after incubation by 60 μl 3 M sodium acetate, 30 μg glycogen, and 990 μl of ice-cold absolute ethanol at −20 °C for at least 1 h. For KBH_4 reduction, 3 μg RNA was incubated with nuclease-free water (mock reaction) or 0.8 M KBH_4 (reduction reaction) at room temperature for 3 h in the dark. RNA samples were then purified by ethanol precipitation. The RNA pellets from both reduction and mock reactions were washed once with 70% ethanol and resuspended in 100 μl aniline-acetate solution (H_2O: glacial acetate acid:aniline, 9:1:1) and incubated at room temperature in the dark for 2 hr to induce cleavage at the m^{7}G site. Then chemical-treated RNA samples were purified by ethanol precipitation and used for Northern blotting and qRT-PCR.

Northern Blotting—The Northern blotting was performed using the NorthernMax™ Kit (AM1940, Invitrogen™) with a few modifications. Briefly, heat-denatured RNA samples were loaded on agarose gels for electrophoresis and then transferred from the agarose gel to the Amersham Hybond-N$^+$ membrane (RPN303B, Cytiva) following the manufacturer's instructions at 4 °C overnight. RNA was then crosslinked to the membrane by 254 nm UV-light, and the blot was hybridized with 20 nM biotin-labeled probe against the 3' fragment of 18s rRNA (Supplementary Table 1). The blot was detected with Amersham™ ECL™ Prime Western Blotting Detection Reagent (RPN2232, Cytiva) after incubation with Streptavidin-HRP (ab7403, Abcam) for 30 min.

RNA Isolation and Purification—Generally, total RNA was extracted from cell lines using QIAzol (79306, Qiagen) according to the manufacturer's instructions. RNA concentration was measured using Thermo Scientific Nanodrop Spectrophotometer. Dynabeads™ Oligo$(dT)_{25}$ (61005, Thermo Fisher Scientific) is used to capture and purify mRNA from total RNA. The mRNA purification procedure was performed twice to deplete all other RNA species. PolyA^+ RNAs were treated with TURBO™ DNase (AM2239, Thermo Fisher Scientific) at 37 °C for 30 min to remove any potential DNA contamination. RNAs were further concentrated using RNA Clean & Concentrator kit (R1014, Zymo Research). Nuclear and cytoplasmic RNAs were extracted from cells using the Fisher BioReagents™ Nuclear or Cytoplasmic RNA Purification Kit (BP280550, Thermo Fisher Scientific). Small RNA (<200 nt) was enriched using mirVana™ miRNA Isolation Kit (AM1560, Thermo Fisher Scientific). Ribosomal RNA (rRNA) was isolated from total RNA using NEBNext rRNA depletion kit (E6310S, New England Biolabs). The RNAs were stored at −80°C and avoided repeated freezing and thawing.

Preparation of RNA or Protein Samples from SG—Previous studies already showed that stressed RNA granule pellet could be a reasonable proxy for full SG preparation,[72] thus we used SG core enriched fraction to validate the enrichment of selected transcripts as well as m^7G modification. To isolate SG core enriched fraction from the whole cell lysate, we refer to several published literature, in which the enrichment of stress granules under stress conditions has been validated.[73,74] After appropriate treatments, one 15 cm-dish cells were washed twice with ice-cold PBS quickly (within 10 s) and then harvested in 1.5 ml ice-cold SG lysis buffer (50 mM Tris pH 7.6, 50 mM NaCl, 5 mM $MgCl_2$, 0.1% NP-40, 1 mM β-mercaptoethanol, 1% EDTA-free protease inhibitor cocktail, and 0.4 U/mL RNase inhibitor) on ice for 20 min. After that, cell suspensions were given 30 strokes in a Dounce homogenizer, followed by centrifugation at 2,000 g for 5 min at 4°C. The supernatant contains cytosolic fraction, and the pellet contains nuclear fraction. Then, 1 ml of the supernatant was centrifuged at 18,000 g for 20 min at 4°C to isolate the insoluble pellet fraction. After discarding the supernatant, the pellet was re-suspended in 1 ml lysis buffer and centrifuged at 18,000 g for another 20 min at 4°C. Then, the supernatant was discarded, whereas the pellet was re-suspended in 300 μl SG lysis buffer and centrifuged at 850 g for 2 min at 4°C. The supernatant represented SG core enriched fractions. The RNAs from cytosolic fraction, nuclear fraction, and SG core-enriched fractions were extracted using QIAzol (79306, Qiagen). The protein concentration of different fractions was normalized by Protein Assay Kits (500-0002EDU, Bio-Rad) and then subjected to Western blotting.

Surface Sensing of Translation (SUnSET)—SUnSET was performed as previously described to detect protein synthesis in HepG2 cell line upon *METTL1* knockout.[75] Briefly, the HepG2 Cas9 single clone was infected with scramble sgRNA and three sgRNAs against *METTL1* (hygromycin-resistant), and the knockout efficiency was validated by Western blotting. Then, cells were seeded in 6-well plate with a density of 1×10^6 cells per well and incubated in DMEM medium supplemented with puromycin (1 μg/ml for HepG2) for indicated time points. The protein sample was extracted at each time point, and western blotting was conducted using anti-puromycin (MABE343, EMD Millipore) as primary antibody. Ponceau S (P7170-1L, Sigma-Aldrich) was used as protein loading control.

Polysome Profiling—The polysome profiling was conducted according to the reported protocol with minor modifications.[76] The HeLa-cas9, HepG2-cas9, and U2OS-cas9 cells were transduced with indicating sgRNA lentivirus and selected with hygromycin (ant-hg-1, Invivogen) for 5–7 days before the experiment. One 15-cm dish of the cells at around 70–80% confluence was used for the polysome profiling. Before collection, cycloheximide (CHX) (C4859, Sigma-Aldrich) was added to the media at 100 μg/ml for 7 min to block active mRNA translation. Then the medium was removed, and the cells were washed with ice-cold PBS (with 100 μg/ml CHX) three times. After centrifugation at 500 g for 5 min, 500 μl lysis buffer (20 mM HEPES pH 7.6, 100 mM KCl, 5 mM $MgCl_2$, 100 μg/ml CHX, 1% Triton X-100, 1% protease inhibitor cocktail, and 40 U/ml RNase inhibitor) was used to resuspend cell pellets and the lysate was kept on ice for 30 min. After incubation, the lysate was centrifuged at 15,000 g for 15 min at 4 °C. Then, 400 μl supernatant was layered on top of a 10% to 50% sucrose gradient (formed by the Gradient Master from BioComp Instruments) containing 20 mM HEPES pH 7.6, 100 mM KCl, 5 mM $MgCl_2$, 100 μg/ml CHX, 1× protease inhibitor, and 20 U/ml RNase inhibitor (EO0382, Thermo Fisher Scientific). The gradient was then centrifuged on an Optima L-100 XP Ultracentrifuge (rotor SW41i) at 41,000 rpm for 2 h at 4 °C. After centrifuge, the sample was fractionated into 20 fractions using the Piston Gradient Fractionator (BioComp Instruments) coupled with a fraction collector (Gilson) and an ECONO UV monitor (BioRad). The A260 absorbance of each fraction was recorded. Part of each fraction was subjected to Western blotting. RNA was purified from fractions using Trizol LS reagent (10-296-010, Thermo Fisher Scientific) and then subjected to RT-qPCR analysis to check the mRNA level of interest gene.

Ribosome profiling (Ribo-seq)—For Ribo-seq, we followed previously reported protocol.[18] Briefly, two 15-cm dishes of U2OS cells with empty vector or QKI7 overexpression were treated with 500 μM $NaAsO_2$ for 1 h before harvesting the cells. Then the medium was removed, and the cells were washed twice with ice-cold PBS. 600 μl lysis buffer (20 mM HEPES, pH 7.6, 100 mM KCl, 5 mM $MgCl_2$, 100 μg/ml CHX, 1% Triton X-100, 1% protease inhibitor cocktail and 40 U/ml RNase inhibitor) was used to lysis the cells and then the lysate was kept on ice for 20 min. After that, triturate the cell ten times through a 26-G needle and then centrifuge at 20,000 g for 15 min. 3 μl Micrococcal Nuclease (M0247S, New England Biolabs) was added in the clear lysate and incubated for 30 min at room temperature with gentle agitation, and 10 μl SUPERase-In RNase Inhibitor (AM2696, Thermo Fisher Scientific) was added to quench the nuclease digestion. Then, 400 μl lysate was loaded to the 10%−50% sucrose density gradient and centrifuged on an Optima L-100 XP Ultracentrifuge (rotor SW41i) at 41,000 rpm for 2 h at 4 °C. After centrifuge, the 80S fraction was collected using the Piston Gradient Fractionator (BioComp Instruments) coupled with a fraction collector (Gilson) and an ECONO UV monitor (BioRad). The RNA samples were purified by using Trizol LS reagent (10-296-010, Thermo Fisher Scientific) accordingly. To purify the ribosome-protected fragments (RPF), the RNA samples were separated on a 15% TBE-Urea Polyacrylamide Gel (EC68852BOX, Thermo Fisher Scientific) and the gel band between 17–34 nt was cut and recovered using Zymo-small RNA page gel recovery kit (R1070, Zymo Research). Before library construction, the end structures of RPF were repaired by T4 polynucleotide kinase (T4 PNK, M0201S, New England Biolabs): 3’ de-phosphorylation: 7 μl RNA sample, 1 μl 10x T4

PNK buffer, 1 μl T4 PNK, 1 μl SUPERase RNase inhibitor were mixed and incubated at 37°C for 1 hour; 5' phosphorylation: 1 μl 10mM ATP and 1 μl extra T4 PNK were added to the reaction mix and then the mixture were kept at 37°C for 30 minutes. The RPF was then purified by Oligo Clean & Concentrator (D4060, Zymo Research). NEBNext small RNA Library Prep Kit (New England BioLabs) was used for library preparation after depletion of rRNA.

Protein Expression and Purification—Protein expression and purification was conducted as previously described with minor modifications.[68–70] The FLAG-tagged QKI5, QKI6 and QKI7 were transiently overexpressed in HEK293T cells. For each protein, four 15-cm dishes of HEK293T cells were lysed in 4 ml lysis buffer (50 mM Tris-HCl pH 7.5, 500 mM NaCl, 1% Triton X-100, 1 mM EDTA, and 1% protease inhibitor), and then rotate for 30 min at 4 °C. Centrifuge at 20,000g for 60 min to clear the cell lysate. The proteins were purified using 100 ul Pierce™ Anti-DYKDDDDK Magnetic Agarose (A36797, Thermo Fisher Scientific) at 4 °C for 4 h. After extensively washed with lysis buffer, proteins were eluted in 100 μl Pierce™ 3x DYKDDDDK Peptide solution (1.25 mg/ml in PBS, A36805, Thermo Fisher Scientific) at 4 °C for 1 h with gentle shaking. The proteins were carefully collected with a magnetic stand. Protein purity was verified with 10% SDS–PAGE and Coomassie blue staining.

Decapping of mRNA—Decapping of mRNA was performed as previously described using Tobacco Decapping Plus 2 (94, Enzymax).[18] A maximum of 6 μg purified polyA$^+$ RNAs were incubated with 5μl 10 × Decapping Reaction Buffer (100 mM Tris-HCl pH 7.5, 1.0 M NaCl, 20 mM $MgCl_2$, and 10 mM DTT), 1 μl 50 mM $MnCl_2$, 2 μl SUPERase-In RNase Inhibitor (AM2696, Thermo Fisher Scientific) and 8 μl Tobacco decapping enzyme in a final volume of 50 μl. For LC-MS/MS sample preparation, 200 ng polyA$^+$ RNAs were treated with 2 μl 10 × Decapping Reaction Buffer and 1 μl Tobacco decapping enzyme in a final volume of 20 μl. The reaction was incubated at 37 °C for 2h. Decapped mRNA was then purified from the solution using Oligo Clean & Concentrator (D4061, Zymo Research).

***In vitro* Transcription—**The 60-mer previously designed RNA oligo[18] sequencing CCAATAAAATATTAACCACCAATAAAATATTAACCAA**G**ATCCACCAATAAAATATTAACC was synthesized using MEGAshortscript T7 Transcription Kit (AM1354, Thermo Fisher Scientific) for 12 h at 37 °C. The DNA template with T7 promoter is synthesized from Integrated DNA Technologies. Either m^{7}GTP (M6133, Sigma-Aldrich) or GTP was used as the unique source of G site in this RNA oligo. After *in vitro* transcription, oligos were further purified using Oligo Clean & Concentrator kit (D4061, Zymo Research).

RNA Pull-down—The 60-mer GTP/m^{7}GTP incorporated RNA oligos were first labeled with biotin using Pierce™ RNA 3' End Biotinylation Kit (20160, Thermo Fisher Scientific). Then, RNA pull-down was conducted using Pierce™ Magnetic RNA Protein Pull Down Kit (20164, Thermo Fisher Scientific) according to the manufacturer's instructions. Briefly, 50 pmol 3' end biotin-labeled GTP/m^{7}GTP incorporated RNA oligos were bound with 50 ul streptavidin magnetic beads in 1×RNA capture buffer for 1h at room temperature with agitation. Streptavidin beads-conjugated GTP/m^{7}GTP RNA oligos were then incubated with

200 μg HepG2 cell lysate or 0.5 μg human recombinant proteins in Protein-RNA binding buffer in a 100 μl final volume overnight at 4 °C. Finally, the beads were washed with 1×washing buffer for four times, and the RNA-protein complexes were eluted using Elution Buffer. Proteins were detected by Western blotting or mass spectrometry analysis.

Fragmented mRNAs Pull-down Assay—Fragmented mRNAs pull-down assay was performed as previously described with some modifications.[77] Briefly, 10 μg mRNA from HeLa cells were fragmented into 100 nt length using NEBNext® Magnesium RNA Fragmentation Module. Then the fragmented mRNA was decapped using Tobacco Decapping Plus 2 enzyme (94, Enzymax) and purified using Oligos Clean & Concentrator (D4061, Zymo Research). One-tenth volume of the supernatant was kept as Input. Then fragmented and cap-depleted mRNAs were incubated with 5μg Flag-QKI5, Flag-QKI6 or Flag-QKI7 proteins in the binding buffer (50 mM Tris-HCl pH 7.5, 250 mM NaCl, 0.4 mM EDTA, 0.1% NP-40, 1 mM DTT, and 0.4 U/μl RNasin) for 1 h on ice. The protein-RNA mixture was then incubated with Pierce™ Anti-DYKDDDDK Magnetic Agarose (A36797, Thermo Fisher Scientific) for 4 h at 4 °C with rotation. After washed four times with binding buffer, the protein-RNA-beads mixture was digested using proteinase K (EO0492, Thermo Fisher Scientific). Both input and immunoprecipitated RNAs were extracted with QIAzol (79306, Qiagen). The recovered RNAs were subjected to UHPLC-QQQ-MS/MS analysis.

RNA Immunoprecipitation (RIP)-seq—For RIP experiment, we followed our protocol as previously described.[69] Briefly, two 15-cm plates of HepG2 or U2OS cells with overexpression of FLAG-tagged QKI5, QKI6 and QKI7 overexpression at 90% confluence were rinsed twice in ice-cold PBS, cross-linked at 254nm (150 mJ/cm^2), collected, and lysed in 1 ml M-PER buffer (78501, Thermo Fisher Scientific) with 100 U/ml RNase inhibitor and 1×protease inhibitor. After kept on ice for 30 min, the cell lysate was sonicated using Bioruptor UCD-200 at 4°C (30s ON, 30s OFF, 10 cycles). Then, the cell lysate was centrifuged at 13,000 rpm for 15 min and the supernatant was collected. One-tenth volume of the supernatant was kept as “input” and the other was subjected to IP. Meanwhile, the 5 μg anti-FLAG antibody (F3165, Sigma-Aldrich) and mouse IgG were conjugated to 50 μl Protein A/G magnetic beads (88803, Thermo Fisher Scientific) and rotated at 4°C for 4 h, followed by washing three times with RIP buffer (150 mM KCl, 25 mM Tris pH 7.4, 5 mM EDTA, 0.5 mM DTT, and 0.5% NP40). Then, the antibody-conjugated Protein A/G beads were incubated with the pre-cleared cell lysate at 4°C overnight. Finally, the protein A/G magnetic beads were washed three times with RIP buffer, and resuspended in 80μl PBS, followed by DNA digestion and protein digestion. Both input and immunoprecipitated RNAs were recovered by using Oligo Clean & Concentrator kit (D4061, Zymo Research). The libraries were constructed using the KAPA Stranded mRNA-Seq Kit (Kapa Biosystems) after depletion of rRNA.

m^{7}G-MeRIP-seq—m^{7}G-MeRIP-seq was conducted by following the previously published protocol.[18] Briefly, 6 μg HepG2 or U2OS mRNA (two round polyA$^+$ purification) was fragmented into 100 nt using NEBNext® Magnesium RNA Fragmentation Module (E6150S, New England Biolabs) following the manufacturer’s protocol. The fragmented mRNA was decapped using Tobacco Decapping Plus 2 enzyme (94, Enzymax). The T4 Polynucleotide

Kinase (EK0032, Thermo Fisher Scientific) was used to repair the end structure of decapped mRNAs and the RNA was purified and concentrated using RNA Clean & Concentrator (R1015, Zymo Research). Then 10% of the repaired and decapped mRNA fragments were kept as "input" group. The other mRNA fragments were incubated with 4 μg anti-m^7G antibody (RN017M, MBL International) in 250 μl 1× IPP buffer (10mM Tris-HCl pH 7.4, 150 mM NaCl, 0.1% NP-40, and freshly added RNase inhibitor), and incubated at 4°C for 4 h with rotation. Then 40 μl pre-cleaned Protein A/G magnetic beads (88803, Thermo Fisher Scientific) were added in the reaction and kept rotation for 4 h at 4 °C. The magnetic beads were then washed four times with 1× IPP buffer. The IP RNA fragments were finally eluted using RNA Clean & Concentrator (R1015, Zymo Research). Both "input" group and "IP" group were prepared for next-generation sequencing. The libraries were constructed with KAPA Stranded mRNA-Seq Kit (Kapa Biosystems).

Bulk RNA-seq—The U2OS cells with empty vector or QKI7 overexpression were treated with 0.5 mM $NaAsO_2$ and total RNAs were extracted using QIAzol (79306, Qiagen) according to the manufacturer's instructions. The RNA concentration was measured by NanoDrop 2000 (Thermo Fisher Scientific), and the RNA integrity was determined by Bioanalyzer (Agilent). The KAPA Stranded mRNA-Seq Kit (Kapa Biosystems) was used for library preparation.

mRNA Stability Profiling—mRNA Stability Profiling (i.e., mRNA stability-sequencing) was performed as previously described with some modifications.[76] Briefly, U2OS cells were seeded into 6-well plates and treated with 5 μg/mL actinomycin D (A9415, Sigma-Aldrich) and 200 μM sodium arsenite (1062771000, Millipore) for 0, 4, and 8 hours. The total RNA was extracted using QIAzol (79306, Qiagen) at indicated time points for RNA-seq. An equal amount of external RNA control consortium (ERCC) RNA spike-in control (Thermo Fisher Scientific) was added to RNA samples as internal controls before library construction. Sequencing libraries were prepared using KAPA Stranded mRNA-Seq Kit (Kapa Biosystems).

QUANTIFICATION AND STATISTICAL ANALYSIS

Data Analysis—For RNA-seq data: Samples were sequenced by Illumina HiSeq 2500 with a single-end 51-bp read length. After sequencing, reads were trimmed for adaptor sequence, masked for low-quality sequence by Cutadapt,[78] and then mapped to GRCh38 reference genome by STAR.[79] Gene expression (RPKM) was calculated by RSEM.[80]

For RIP-seq data: Samples were sequenced by Illumina HiSeq 2500 or NovaSeq 6000 platform. After sequencing, all reads were mapped to GRCh38 reference genome by STAR.[79] The RNA-protein binding locations were calculated using exomePeak,[81] and the motif was enriched by using HOMER software with default RNA analysis parameters.[82] The potential targets were identified and enriched using MSigDB,[83] and the transcriptome-wide distribution of target transcripts was generated using metaPlotR.[84] The circos plots were generated using Circos software.[85] The KEGG pathway enrichment analysis was performed using David bioinformatics resources (v6.8).[86]

For m^7G MeRIP-seq data: Samples were sequenced by Illumina HiSeq 2500 with a single-end 51-bp read length. All the reads from both input and m^7G IP samples were mapped to GRCh38 reference genome by STAR.[79] The m^7G peaks were calculated using exomePeak,[81] and the motif was enriched by using HOMER software with default RNA analysis parameters.[82] The distribution of m7G peaks was generated using metaPlotR.[84]

For mRNA stability profiling: Samples were sequenced by Illumina NovaSeq 6000 platform. After sequencing, reads were trimmed for adaptor sequence, masked for low-quality sequence by Cutadapt,[78] and then mapped to GRCh38 reference genome by STAR.[79] Gene expression (RPKM) was calculated by RSEM.[80] The turnover rate and half-life of mRNA was calculated according to a previously published paper.[87] As actinomycin D treatment results in transcription stalling, the change of mRNA concentration at a given time (*dC/dt*) is proportional to the constant of mRNA decay (k_{decay}) and mRNA concentration (C) as shown in the following equation:

$$dC/dt = -k_{decay}C$$

Thus, the mRNA degradation rate K_{decay} was estimated by:

$$\mathrm{In}(C/C_0) = -k_{decay}t$$

When 50% of mRNA is decayed (i.e., $C/C_0 = 1/2$), the equation below can be used to calculate the mRNA half-life ($t_{1/2}$):

$$\mathrm{In}\,(1/2) = -k_{decay}t_{1/2}$$

from where:

$$t_{1/2} = ln2/k_{decay}$$

For Ribo-seq: Samples were sequenced by Illumina HiSeq 2500 with a single-end 51-bp read length. All the reads were quality-based trimmed and the adaptors were removed using Cutadapt.[78] The reads (with minimum-length 16nts) were mapped to GRCh38 reference genome using STAR.[79] Then the ribosome profiling was analyzed by RSEM.[80] Only genes with expression ≥ 0.01 (including both input abundance and ribosome profiling abundance) in both empty vector and QKI7 overexpression group were selected for further analysis. Translation efficiency (TE) was calculated by the ratio of (normalized ribosome profiling abundance+1)/(normalized input RNA abundance+1). For upregulated and downregulated transcripts, the cut-off value is $|\log_{1.5}(\mathrm{QKI7/EV})|>0.5$.

Statistical Analysis—Data are presented as mean ± standard error of the mean (SEM). Statistical comparisons were performed by using two-tailed *t*-tests, one-way ANOVA, two-way ANOVA, Hypergeometric test, Person's chi-square test or Extra-sum-of-squares F test as indicated in the figure legends. Pearson tests were performed for correlation analysis. *P* values less than 0.05 were considered statistically significant. NS, not significant. All

statistical analyses were carried out using Graphpad Prism 8 (GraphPad Software). For all violin plots, minimum, 25th percentage, medium, 75th percentage and maximum values are shown. Intensity of fluorescence were analyzed using ZEN Black software (Zeiss). Each sequence RNA sample (RIP-seq, m^{7}G MeRIP-seq, Ribo-seq, mRNA Stability Profiling and bulk RNA-seq) has two biological replicates. For other experiments, the number of replicates is indicated in the figure legends. All western blotting, northern blotting, dot blot and immunofluorescence images are representative of three independent experiments.

Supplementary Material

Refer to Web version on PubMed Central for supplementary material.

Acknowledgments

This work was supported in part by the U.S. National Institutes of Health (NIH) grants R01 CA271497 (J.C.), R01 CA243386 (J.C.), R01 CA214965 (J.C.), R01 CA236399 (J.C.), R01 CA211614 (J.C.), R01 DK124116 (J.C), T32 CA186895 (B.T), The Simms/Mann Family Foundation (J.C.), The Margaret E. Early Medical Research Trust (R.S.), the Shared Resources Pilot Program at City of Hope (R.S.), AASLD Foundation PNC22-261362 (R.S.), and Leukemia Research Foundation (R.S.). J.C. is a Leukemia & Lymphoma Society (LLS) Scholar.

References

1. Boccaletto P, Stefaniak F, Ray A, Cappannini A, Mukherjee S, Purta E, Kurkowska M, Shirvanizadeh N, Destefanis E, Groza P, et al. (2022). MODOMICS: a database of RNA modification pathways. 2021 update. Nucleic Acids Res 50, D231–D235. 10.1093/nar/gkab1083. [PubMed: 34893873]
2. Roundtree IA, Evans ME, Pan T, and He C (2017). Dynamic RNA Modifications in Gene Expression Regulation. Cell 169, 1187–1200. 10.1016/j.cell.2017.05.045. [PubMed: 28622506]
3. Huang H, Weng H, and Chen J (2020). m(6)A Modification in Coding and Non-coding RNAs: Roles and Therapeutic Implications in Cancer. Cancer Cell 37, 270–288. 10.1016/j.ccell.2020.02.004. [PubMed: 32183948]
4. Shatkin AJ (1976). Capping of eucaryotic mRNAs. Cell 9, 645–653. 10.1016/0092-8674(76)90128-8. [PubMed: 1017010]
5. Mandal SS, Chu C, Wada T, Handa H, Shatkin AJ, and Reinberg D (2004). Functional interactions of RNA-capping enzyme with factors that positively and negatively regulate promoter escape by RNA polymerase II. Proc Natl Acad Sci U S A 101, 7572–7577. 10.1073/pnas.0401493101. [PubMed: 15136722]
6. Ramanathan A, Robb GB, and Chan SH (2016). mRNA capping: biological functions and applications. Nucleic Acids Res 44, 7511–7526. 10.1093/nar/gkw551. [PubMed: 27317694]
7. Lin S, Liu Q, Lelyveld VS, Choe J, Szostak JW, and Gregory RI (2018). Mettl1/Wdr4-Mediated m(7)G tRNA Methylome Is Required for Normal mRNA Translation and Embryonic Stem Cell Self-Renewal and Differentiation. Mol Cell 71, 244–255 e245. 10.1016/j.molcel.2018.06.001. [PubMed: 29983320]
8. White J, Li Z, Sardana R, Bujnicki JM, Marcotte EM, and Johnson AW (2008). Bud23 methylates G1575 of 18S rRNA and is required for efficient nuclear export of pre-40S subunits. Mol Cell Biol 28, 3151–3161. 10.1128/MCB.01674-07. [PubMed: 18332120]
9. Alexandrov A, Martzen MR, and Phizicky EM (2002). Two proteins that form a complex are required for 7-methylguanosine modification of yeast tRNA. RNA 8, 1253–1266. 10.1017/s1355838202024019. [PubMed: 12403464]
10. Orellana EA, Liu Q, Yankova E, Pirouz M, De Braekeleer E, Zhang W, Lim J, Aspris D, Sendinc E, Garyfallos DA, et al. (2021). METTL1-mediated m(7)G modification of Arg-TCT tRNA drives oncogenic transformation. Mol Cell 81, 3323–3338 e3314. 10.1016/j.molcel.2021.06.031. [PubMed: 34352207]

11. Dai Z, Liu H, Liao J, Huang C, Ren X, Zhu W, Zhu S, Peng B, Li S, Lai J, et al. (2021). N(7)-Methylguanosine tRNA modification enhances oncogenic mRNA translation and promotes intrahepatic cholangiocarcinoma progression. Mol Cell 81, 3339–3355 e3338. 10.1016/j.molcel.2021.07.003. [PubMed: 34352206]
12. Zorbas C, Nicolas E, Wacheul L, Huvelle E, Heurgue-Hamard V, and Lafontaine DL (2015). The human 18S rRNA base methyltransferases DIMT1L and WBSCR22-TRMT112 but not rRNA modification are required for ribosome biogenesis. Mol Biol Cell 26, 2080–2095. 10.1091/mbc.E15-02-0073. [PubMed: 25851604]
13. Pandolfini L, Barbieri I, Bannister AJ, Hendrick A, Andrews B, Webster N, Murat P, Mach P, Brandi R, Robson SC, et al. (2019). METTL1 Promotes let-7 MicroRNA Processing via m7G Methylation. Mol Cell 74, 1278–1290 e1279. 10.1016/j.molcel.2019.03.040. [PubMed: 31031083]
14. Chu JM, Ye TT, Ma CJ, Lan MD, Liu T, Yuan BF, and Feng YQ (2018). Existence of Internal N7-Methylguanosine Modification in mRNA Determined by Differential Enzyme Treatment Coupled with Mass Spectrometry Analysis. ACS Chem Biol 13, 3243–3250. 10.1021/acschembio.7b00906. [PubMed: 29313662]
15. Zhang LS, Liu C, and He C (2021). Transcriptome-Wide Detection of Internal N(7)-Methylguanosine. Methods Mol Biol 2298, 97–104. 10.1007/978-1-0716-1374-0_6. [PubMed: 34085240]
16. Enroth C, Poulsen LD, Iversen S, Kirpekar F, Albrechtsen A, and Vinther J (2019). Detection of internal N7-methylguanosine (m7G) RNA modifications by mutational profiling sequencing. Nucleic Acids Res 47, e126. 10.1093/nar/gkz736. [PubMed: 31504776]
17. Malbec L, Zhang T, Chen YS, Zhang Y, Sun BF, Shi BY, Zhao YL, Yang Y, and Yang YG (2019). Dynamic methylome of internal mRNA N(7)-methylguanosine and its regulatory role in translation. Cell Res 29, 927–941. 10.1038/s41422-019-0230-z. [PubMed: 31520064]
18. Zhang LS, Liu C, Ma H, Dai Q, Sun HL, Luo G, Zhang Z, Zhang L, Hu L, Dong X, and He C (2019). Transcriptome-wide Mapping of Internal N(7)-Methylguanosine Methylome in Mammalian mRNA. Mol Cell 74, 1304–1316 e1308. 10.1016/j.molcel.2019.03.036. [PubMed: 31031084]
19. Khong A, Matheny T, Jain S, Mitchell SF, Wheeler JR, and Parker R (2017). The Stress Granule Transcriptome Reveals Principles of mRNA Accumulation in Stress Granules. Mol Cell 68, 808–820 e805. 10.1016/j.molcel.2017.10.015. [PubMed: 29129640]
20. Gao X, Jiang L, Gong Y, Chen X, Ying M, Zhu H, He Q, Yang B, and Cao J (2019). Stress granule: A promising target for cancer treatment. Br J Pharmacol 176, 4421–4433. 10.1111/bph.14790. [PubMed: 31301065]
21. Ivanov P, Kedersha N, and Anderson P (2019). Stress Granules and Processing Bodies in Translational Control. Cold Spring Harb Perspect Biol 11. 10.1101/cshperspect.a032813.
22. Fu Y, and Zhuang X (2020). m(6)A-binding YTHDF proteins promote stress granule formation. Nat Chem Biol 16, 955–963. 10.1038/s41589-020-0524-y. [PubMed: 32451507]
23. Ries RJ, Zaccara S, Klein P, Olarerin-George A, Namkoong S, Pickering BF, Patil DP, Kwak H, Lee JH, and Jaffrey SR (2019). m(6)A enhances the phase separation potential of mRNA. Nature 571, 424–428. 10.1038/s41586-019-1374-1. [PubMed: 31292544]
24. Anders M, Chelysheva I, Goebel I, Trenkner T, Zhou J, Mao Y, Verzini S, Qian SB, and Ignatova Z (2018). Dynamic m(6)A methylation facilitates mRNA triaging to stress granules. Life Sci Alliance 1, e201800113. 10.26508/lsa.201800113. [PubMed: 30456371]
25. Vernet C, and Artzt K (1997). STAR, a gene family involved in signal transduction and activation of RNA. Trends Genet 13, 479–484. 10.1016/s0168-9525(97)01269-9. [PubMed: 9433137]
26. Darbelli L, and Richard S (2016). Emerging functions of the Quaking RNA-binding proteins and link to human diseases. Wiley Interdiscip Rev RNA 7, 399–412. 10.1002/wrna.1344. [PubMed: 26991871]
27. Wu J, Zhou L, Tonissen K, Tee R, and Artzt K (1999). The quaking I-5 protein (QKI-5) has a novel nuclear localization signal and shuttles between the nucleus and the cytoplasm. J Biol Chem 274, 29202–29210. 10.1074/jbc.274.41.29202. [PubMed: 10506177]

28. Pilotte J, Larocque D, and Richard S (2001). Nuclear translocation controlled by alternatively spliced isoforms inactivates the QUAKING apoptotic inducer. Genes Dev 15, 845–858. 10.1101/gad.860301. [PubMed: 11297509]
29. Li ZZ, Kondo T, Murata T, Ebersole TA, Nishi T, Tada K, Ushio Y, Yamamura K, and Abe K (2002). Expression of Hqk encoding a KH RNA binding protein is altered in human glioma. Jpn J Cancer Res 93, 167–177. 10.1111/j.1349-7006.2002.tb01255.x. [PubMed: 11856480]
30. Boulias K, and Greer EL (2019). Put the Pedal to the METTL1: Adding Internal m(7)G Increases mRNA Translation Efficiency and Augments miRNA Processing. Mol Cell 74, 1105–1107. 10.1016/j.molcel.2019.06.004. [PubMed: 31226274]
31. Li JH, Liu S, Zhou H, Qu LH, and Yang JH (2014). starBase v2.0: decoding miRNA-ceRNA, miRNA-ncRNA and protein-RNA interaction networks from large-scale CLIP-Seq data. Nucleic Acids Res 42, D92–97. 10.1093/nar/gkt1248. [PubMed: 24297251]
32. Ruzzenente B, Metodiev MD, Wredenberg A, Bratic A, Park CB, Camara Y, Milenkovic D, Zickermann V, Wibom R, Hultenby K, et al. (2012). LRPPRC is necessary for polyadenylation and coordination of translation of mitochondrial mRNAs. EMBO J 31, 443–456. 10.1038/emboj.2011.392. [PubMed: 22045337]
33. Cui J, Wang L, Ren X, Zhang Y, and Zhang H (2019). LRPPRC: A Multifunctional Protein Involved in Energy Metabolism and Human Disease. Front Physiol 10, 595. 10.3389/fphys.2019.00595. [PubMed: 31178748]
34. Van Nostrand EL, Pratt GA, Yee BA, Wheeler EC, Blue SM, Mueller J, Park SS, Garcia KE, Gelboin-Burkhart C, Nguyen TB, et al. (2020). Principles of RNA processing from analysis of enhanced CLIP maps for 150 RNA binding proteins. Genome Biol 21, 90. 10.1186/s13059-020-01982-9. [PubMed: 32252787]
35. Galarneau A, and Richard S (2005). Target RNA motif and target mRNAs of the Quaking STAR protein. Nat Struct Mol Biol 12, 691–698. 10.1038/nsmb963. [PubMed: 16041388]
36. Teplova M, Hafner M, Teplov D, Essig K, Tuschl T, and Patel DJ (2013). Structure-function studies of STAR family Quaking proteins bound to their in vivo RNA target sites. Genes Dev 27, 928–940. 10.1101/gad.216531.113. [PubMed: 23630077]
37. Liu J, Dou X, Chen C, Chen C, Liu C, Xu MM, Zhao S, Shen B, Gao Y, Han D, and He C (2020). N (6)-methyladenosine of chromosome-associated regulatory RNA regulates chromatin state and transcription. Science 367, 580–586. 10.1126/science.aay6018. [PubMed: 31949099]
38. Wang L, Hui H, Agrawal K, Kang Y, Li N, Tang R, Yuan J, and Rana TM (2020). m(6) A RNA methyltransferases METTL3/14 regulate immune responses to anti-PD-1 therapy. EMBO J 39, e104514. 10.15252/embj.2020104514. [PubMed: 32964498]
39. Su R, Dong L, Li Y, Gao M, He PC, Liu W, Wei J, Zhao Z, Gao L, Han L, et al. (2022). METTL16 exerts an m(6)A-independent function to facilitate translation and tumorigenesis. Nat Cell Biol 24, 205–216. 10.1038/s41556-021-00835-2. [PubMed: 35145225]
40. Anderson P, and Kedersha N (2009). RNA granules: post-transcriptional and epigenetic modulators of gene expression. Nat Rev Mol Cell Biol 10, 430–436. 10.1038/nrm2694. [PubMed: 19461665]
41. Warde-Farley D, Donaldson SL, Comes O, Zuberi K, Badrawi R, Chao P, Franz M, Grouios C, Kazi F, Lopes CT, et al. (2010). The GeneMANIA prediction server: biological network integration for gene prioritization and predicting gene function. Nucleic Acids Res 38, W214–220. 10.1093/nar/gkq537. [PubMed: 20576703]
42. Montojo J, Zuberi K, Rodriguez H, Kazi F, Wright G, Donaldson SL, Morris Q, and Bader GD (2010). GeneMANIA Cytoscape plugin: fast gene function predictions on the desktop. Bioinformatics 26, 2927–2928. 10.1093/bioinformatics/btq562. [PubMed: 20926419]
43. Yang P, Mathieu C, Kolaitis RM, Zhang P, Messing J, Yurtsever U, Yang Z, Wu J, Li Y, Pan Q, et al. (2020). G3BP1 Is a Tunable Switch that Triggers Phase Separation to Assemble Stress Granules. Cell 181, 325–345 e328. 10.1016/j.cell.2020.03.046. [PubMed: 32302571]
44. Singleton RS, Liu-Yi P, Formenti F, Ge W, Sekirnik R, Fischer R, Adam J, Pollard PJ, Wolf A, Thalhammer A, et al. (2014). OGFOD1 catalyzes prolyl hydroxylation of RPS23 and is involved in translation control and stress granule formation. Proc Natl Acad Sci U S A 111, 4031–4036. 10.1073/pnas.1314482111. [PubMed: 24550447]

45. Wang B, Maxwell BA, Joo JH, Gwon Y, Messing J, Mishra A, Shaw TI, Ward AL, Quan H, Sakurada SM, et al. (2019). ULK1 and ULK2 Regulate Stress Granule Disassembly Through Phosphorylation and Activation of VCP/p97. Mol Cell 74, 742–757 e748. 10.1016/j.molcel.2019.03.027. [PubMed: 30979586]
46. Matheny T, Van Treeck B, Huynh TN, and Parker R (2021). RNA partitioning into stress granules is based on the summation of multiple interactions. RNA 27, 174–189. 10.1261/rna.078204.120. [PubMed: 33199441]
47. Moon SL, Morisaki T, Khong A, Lyon K, Parker R, and Stasevich TJ (2019). Multicolour single-molecule tracking of mRNA interactions with RNP granules. Nat Cell Biol 21, 162–168. 10.1038/s41556-018-0263-4. [PubMed: 30664789]
48. Wilbertz JH, Voigt F, Horvathova I, Roth G, Zhan Y, and Chao JA (2019). Single-Molecule Imaging of mRNA Localization and Regulation during the Integrated Stress Response. Mol Cell 73, 946–958 e947. 10.1016/j.molcel.2018.12.006. [PubMed: 30661979]
49. Kimball SR, Horetsky RL, Ron D, Jefferson LS, and Harding HP (2003). Mammalian stress granules represent sites of accumulation of stalled translation initiation complexes. Am J Physiol Cell Physiol 284, C273–284. 10.1152/ajpcell.00314.2002. [PubMed: 12388085]
50. Harvey R, Dezi V, Pizzinga M, and Willis AE (2017). Post-transcriptional control of gene expression following stress: the role of RNA-binding proteins. Biochem Soc Trans 45, 1007–1014. 10.1042/BST20160364. [PubMed: 28710288]
51. Kedersha N, Panas MD, Achorn CA, Lyons S, Tisdale S, Hickman T, Thomas M, Lieberman J, McInerney GM, and Ivanov P (2016). G3BP–Caprin1–USP10 complexes mediate stress granule condensation and associate with 40S subunits. J Cell Biol 212. 10.1083/jcb.201508028.
52. Panas MD, Ivanov P, and Anderson P (2016). Mechanistic insights into mammalian stress granule dynamics. J Cell Biol 215, 313–323. 10.1083/jcb.201609081. [PubMed: 27821493]
53. Anderson P, Kedersha N, and Ivanov P (2015). Stress granules, P-bodies and cancer. Biochim Biophys Acta 1849, 861–870. 10.1016/j.bbagrm.2014.11.009. [PubMed: 25482014]
54. Zhan Y, Wang H, Ning Y, Zheng H, Liu S, Yang Y, Zhou M, and Fan S (2020). Understanding the roles of stress granule during chemotherapy for patients with malignant tumors. Am J Cancer Res 10, 2226–2241. [PubMed: 32905441]
55. Domoto T, Pyko IV, Furuta T, Miyashita K, Uehara M, Shimasaki T, Nakada M, and Minamoto T (2016). Glycogen synthase kinase-3beta is a pivotal mediator of cancer invasion and resistance to therapy. Cancer Sci 107, 1363–1372. 10.1111/cas.13028. [PubMed: 27486911]
56. Nguyen CDK, and Yi C (2019). YAP/TAZ Signaling and Resistance to Cancer Therapy. Trends in cancer 5, 283–296. 10.1016/j.trecan.2019.02.010. [PubMed: 31174841]
57. Zeng R, and Dong J (2021). The Hippo Signaling Pathway in Drug Resistance in Cancer. Cancers (Basel) 13. 10.3390/cancers13020318.
58. Qiu Z, Li H, Zhang Z, Zhu Z, He S, Wang X, Wang P, Qin J, Zhuang L, Wang W, et al. (2019). A Pharmacogenomic Landscape in Human Liver Cancers. Cancer Cell 36, 179–193 e111. 10.1016/j.ccell.2019.07.001. [PubMed: 31378681]
59. Buchan JR, and Parker R (2009). Eukaryotic stress granules: the ins and outs of translation. Mol Cell 36, 932–941. 10.1016/j.molcel.2009.11.020. [PubMed: 20064460]
60. Anderson P, and Kedersha N (2008). Stress granules: the Tao of RNA triage. Trends Biochem Sci 33, 141–150. 10.1016/j.tibs.2007.12.003. [PubMed: 18291657]
61. Zahir N, Sun R, Gallahan D, Gatenby RA, and Curtis C (2020). Characterizing the ecological and evolutionary dynamics of cancer. Nat Genet 52, 759–767. 10.1038/s41588-020-0668-4. [PubMed: 32719518]
62. Bittencourt L, Negreiros-Lima G, Sousa L, Silva A, Souza I, Ribeiro R, Dutra M, Silva R, Dias A, and Soriani F (2019). G3BP1 knockdown sensitizes U87 glioblastoma cell line to Bortezomib by inhibiting stress granules assembly and potentializing apoptosis. Journal of neuro-oncology 144, 463–473. 10.1007/s11060-019-03252-6. [PubMed: 31392596]
63. Mukhopadhyay S, Goswami D, Adiseshaiah PP, Burgan W, Yi M, Guerin TM, Kozlov SV, Nissley DV, and McCormick F (2020). Undermining Glutaminolysis Bolsters Chemotherapy While NRF2 Promotes Chemoresistance in KRAS-Driven Pancreatic Cancers. Cancer Res 80, 1630–1643. 10.1158/0008-5472.CAN-19-1363. [PubMed: 31911550]

64. Conn SJ, Pillman KA, Toubia J, Conn VM, Salmanidis M, Phillips CA, Roslan S, Schreiber AW, Gregory PA, and Goodall GJ (2015). The RNA binding protein quaking regulates formation of circRNAs. Cell 160, 1125–1134. 10.1016/j.cell.2015.02.014. [PubMed: 25768908]

65. Chen X, Liu Y, Xu C, Ba L, Liu Z, Li X, Huang J, Simpson E, Gao H, Cao D, et al. (2021). QKI is a critical pre-mRNA alternative splicing regulator of cardiac myofibrillogenesis and contractile function. Nat Commun 12, 89. 10.1038/s41467-020-20327-5. [PubMed: 33397958]

66. Wang Y, Vogel G, Yu Z, and Richard S (2013). The QKI-5 and QKI-6 RNA binding proteins regulate the expression of microRNA 7 in glial cells. Mol Cell Biol 33, 1233–1243. 10.1128/MCB.01604-12. [PubMed: 23319046]

67. Soderberg O, Leuchowius KJ, Gullberg M, Jarvius M, Weibrecht I, Larsson LG, and Landegren U (2008). Characterizing proteins and their interactions in cells and tissues using the in situ proximity ligation assay. Methods 45, 227–232. 10.1016/j.ymeth.2008.06.014. [PubMed: 18620061]

68. Su R, Dong L, Li C, Nachtergaele S, Wunderlich M, Qing Y, Deng X, Wang Y, Weng X, Hu C, et al. (2018). R-2HG Exhibits Anti-tumor Activity by Targeting FTO/m(6)A/MYC/CEBPA Signaling. Cell 172, 90–105 e123. 10.1016/j.cell.2017.11.031. [PubMed: 29249359]

69. Su R, Dong L, Li Y, Gao M, Han L, Wunderlich M, Deng X, Li H, Huang Y, Gao L, et al. (2020). Targeting FTO Suppresses Cancer Stem Cell Maintenance and Immune Evasion. Cancer Cell 38, 79–96 e11. 10.1016/j.ccell.2020.04.017. [PubMed: 32531268]

70. Huang H, Weng H, Sun W, Qin X, Shi H, Wu H, Zhao BS, Mesquita A, Liu C, Yuan CL, et al. (2018). Recognition of RNA N(6)-methyladenosine by IGF2BP proteins enhances mRNA stability and translation. Nat Cell Biol 20, 285–295. 10.1038/s41556-018-0045-z. [PubMed: 29476152]

71. Zhang LS, Ju CW, Liu C, Wei J, Dai Q, Chen L, Ye C, and He C (2022). m(7)G-quant-seq: Quantitative Detection of RNA Internal N(7)-Methylguanosine. ACS Chem Biol 17, 3306–3312. 10.1021/acschembio.2c00792. [PubMed: 36398936]

72. Matheny T, Rao BS, and Parker R (2019). Transcriptome-Wide Comparison of Stress Granules and P-Bodies Reveals that Translation Plays a Major Role in RNA Partitioning. Mol Cell Biol 39, e00313–00319. 10.1128/MCB.00313-19. [PubMed: 31591142]

73. Namkoong S, Ho A, Woo YM, Kwak H, and Lee JH (2018). Systematic Characterization of Stress-Induced RNA Granulation. Mol Cell 70, 175–187 e178. 10.1016/j.molcel.2018.02.025. [PubMed: 29576526]

74. Khong A, Jain S, Matheny T, Wheeler JR, and Parker R (2018). Isolation of mammalian stress granule cores for RNA-Seq analysis. Methods 137, 49–54. 10.1016/j.ymeth.2017.11.012. [PubMed: 29196162]

75. Schmidt EK, Clavarino G, Ceppi M, and Pierre P (2009). SUnSET, a nonradioactive method to monitor protein synthesis. Nat Methods 6, 275–277. 10.1038/nmeth.1314. [PubMed: 19305406]

76. Shen C, Sheng Y, Zhu AC, Robinson S, Jiang X, Dong L, Chen H, Su R, Yin Z, Li W, et al. (2020). RNA Demethylase ALKBH5 Selectively Promotes Tumorigenesis and Cancer Stem Cell Self-Renewal in Acute Myeloid Leukemia. Cell Stem Cell 27, 64–80 e69. 10.1016/j.stem.2020.04.009. [PubMed: 32402250]

77. Yang X, Yang Y, Sun BF, Chen YS, Xu JW, Lai WY, Li A, Wang X, Bhattarai DP, Xiao W, et al. (2017). 5-methylcytosine promotes mRNA export - NSUN2 as the methyltransferase and ALYREF as an m(5)C reader. Cell Res 27, 606–625. 10.1038/cr.2017.55. [PubMed: 28418038]

78. Martin M (2011). Cutadapt removes adapter sequences from high-throughput sequencing reads. EMBnet. journal 17, 10–12. 10.14806/ej.17.1.200.

79. Dobin A, Davis CA, Schlesinger F, Drenkow J, Zaleski C, Jha S, Batut P, Chaisson M, and Gingeras TR (2013). STAR: ultrafast universal RNA-seq aligner. Bioinformatics 29, 15–21. 10.1093/bioinformatics/bts635. [PubMed: 23104886]

80. Li B, and Dewey CN (2011). RSEM: accurate transcript quantification from RNA-Seq data with or without a reference genome. BMC Bioinformatics 12, 323. 10.1186/1471-2105-12-323. [PubMed: 21816040]

81. Meng J, Lu Z, Liu H, Zhang L, Zhang S, Chen Y, Rao MK, and Huang Y (2014). A protocol for RNA methylation differential analysis with MeRIP-Seq data and exomePeak R/Bioconductor package. Methods 69, 274–281. 10.1016/j.ymeth.2014.06.008. [PubMed: 24979058]

82. Heinz S, Benner C, Spann N, Bertolino E, Lin YC, Laslo P, Cheng JX, Murre C, Singh H, and Glass CK (2010). Simple combinations of lineage-determining transcription factors prime cis-regulatory elements required for macrophage and B cell identities. Mol Cell 38, 576–589. 10.1016/j.molcel.2010.05.004. [PubMed: 20513432]

83. Liberzon A, Subramanian A, Pinchback R, Thorvaldsdottir H, Tamayo P, and Mesirov JP (2011). Molecular signatures database (MSigDB) 3.0. Bioinformatics 27, 1739–1740. 10.1093/bioinformatics/btr260. [PubMed: 21546393]

84. Olarerin-George AO, and Jaffrey SR (2017). MetaPlotR: a Perl/R pipeline for plotting metagenes of nucleotide modifications and other transcriptomic sites. Bioinformatics 33, 1563–1564. 10.1093/bioinformatics/btx002. [PubMed: 28158328]

85. Krzywinski M, Schein J, Birol I, Connors J, Gascoyne R, Horsman D, Jones SJ, and Marra MA (2009). Circos: an information aesthetic for comparative genomics. Genome research 19, 1639–1645. 10.1101/gr.092759.109. [PubMed: 19541911]

86. Huang da W, Sherman BT, and Lempicki RA (2009). Bioinformatics enrichment tools: paths toward the comprehensive functional analysis of large gene lists. Nucleic Acids Res 37, 1–13. 10.1093/nar/gkn923. [PubMed: 19033363]

87. Chen CY, Ezzeddine N, and Shyu AB (2008). Messenger RNA half-life measurements in mammalian cells. Methods Enzymol 448, 335–357. 10.1016/S0076-6879(08)02617-7. [PubMed: 19111184]

88. Cheng Z, Gong Y, Ma Y, Lu K, Lu X, Pierce LA, Thompson RC, Muller S, Knapp S, and Wang J (2013). Inhibition of BET bromodomain targets genetically diverse glioblastoma. Clin Cancer Res 19, 1748–1759. 10.1158/1078-0432.CCR-12-3066. [PubMed: 23403638]

89. Sanjana NE, Shalem O, and Zhang F (2014). Improved vectors and genome-wide libraries for CRISPR screening. Nat Methods 11, 783–784. 10.1038/nmeth.3047. [PubMed: 25075903]

90. Stringer BW, Day BW, D'Souza RCJ, Jamieson PR, Ensbey KS, Bruce ZC, Lim YC, Goasdoue K, Offenhauser C, Akgul S, et al. (2019). A reference collection of patient-derived cell line and xenograft models of proneural, classical and mesenchymal glioblastoma. Sci Rep 9, 4902. 10.1038/s41598-019-41277-z. [PubMed: 30894629]

91. Dull T, Zufferey R, Kelly M, Mandel RJ, Nguyen M, Trono D, and Naldini L (1998). A third-generation lentivirus vector with a conditional packaging system. J Virol 72, 8463–8471. 10.1128/JVI.72.11.8463-8471.1998. [PubMed: 9765382]

92. Stewart SA, Dykxhoorn DM, Palliser D, Mizuno H, Yu EY, An DS, Sabatini DM, Chen IS, Hahn WC, Sharp PA, et al. (2003). Lentivirus-delivered stable gene silencing by RNAi in primary cells. RNA 9, 493–501. 10.1261/rna.2192803. [PubMed: 12649500]

Highlights

- Quaking proteins (QKIs) bind to internal m^7G-modified mRNAs with GA-rich motifs
- QKI7 interacts with G3BP1, a stress granule protein
- QKI7 shuttles internal m^7G-modified mRNAs into stress granules under stress conditions
- QKI7 regulates mRNA metabolism and sensitizes cancer cells to chemotherapy drugs

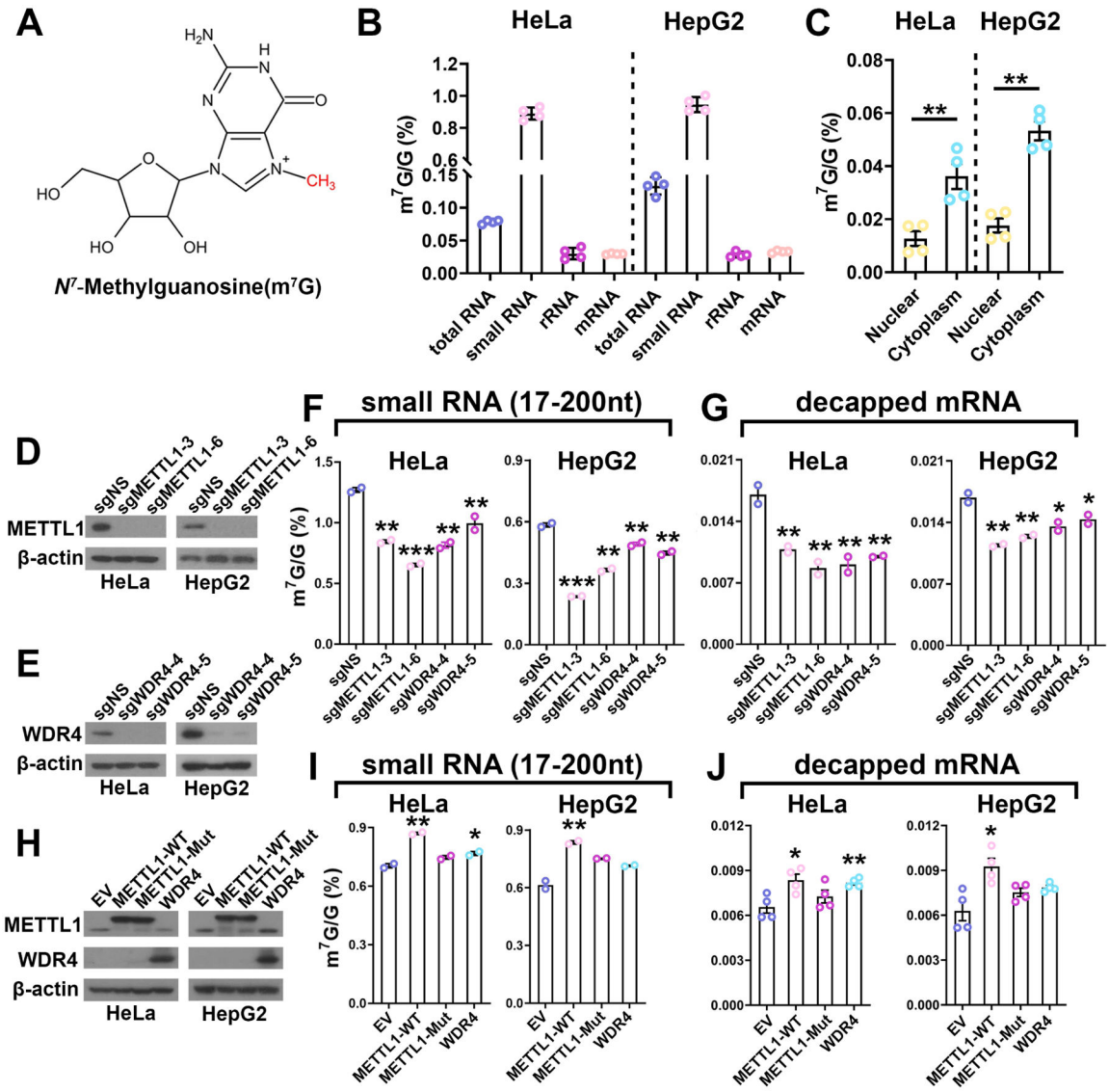

Figure 1. Distribution and quantitation of internal m^{7}G modification in mRNA

(A) The chemical structure of m^{7}G methylation.

(B-C) The internal m^{7}G/G levels in various RNAs (B) and the nuclear and cytoplasmic cap-depleted polyA$^+$ RNAs (C), as detected by LC-MS/MS.

(D-E) *METTL1* (D) and *WDR4* (E) KO efficacy in HeLa and HepG2 Cas9 single clones.

(F-G) LC-MS/MS quantification of internal m^{7}G abundance changes in small RNA (F) and cap-depleted polyA$^+$ mRNA (G) isolated from HeLa and HepG2 cells upon *METTL1* or *WDR4* KO.

(H) Validation of wild-type METTL1 (METTL1-WT), catalytically inactive METTL1 (METTL1-Mut), or WDR4 overexpression in HeLa and HepG2 cells.

(I-J) LC-MS/MS quantification of internal m^{7}G abundance changes in small RNA (I) and cap-depleted polyA$^+$ mRNA (J) isolated from HeLa and HepG2 cells upon METTL1 and WDR4 overexpression.

Two-tailed student's t-test (C); One-way ANOVA (F, G, I, J). *$p < 0.05$; **$p < 0.01$; ***$p < 0.001$. Data in B, C, and J are presented as mean ± SEM (n = 4); Data in F, G, and I are presented as mean ± SEM (n = 2). See also Figure S1.

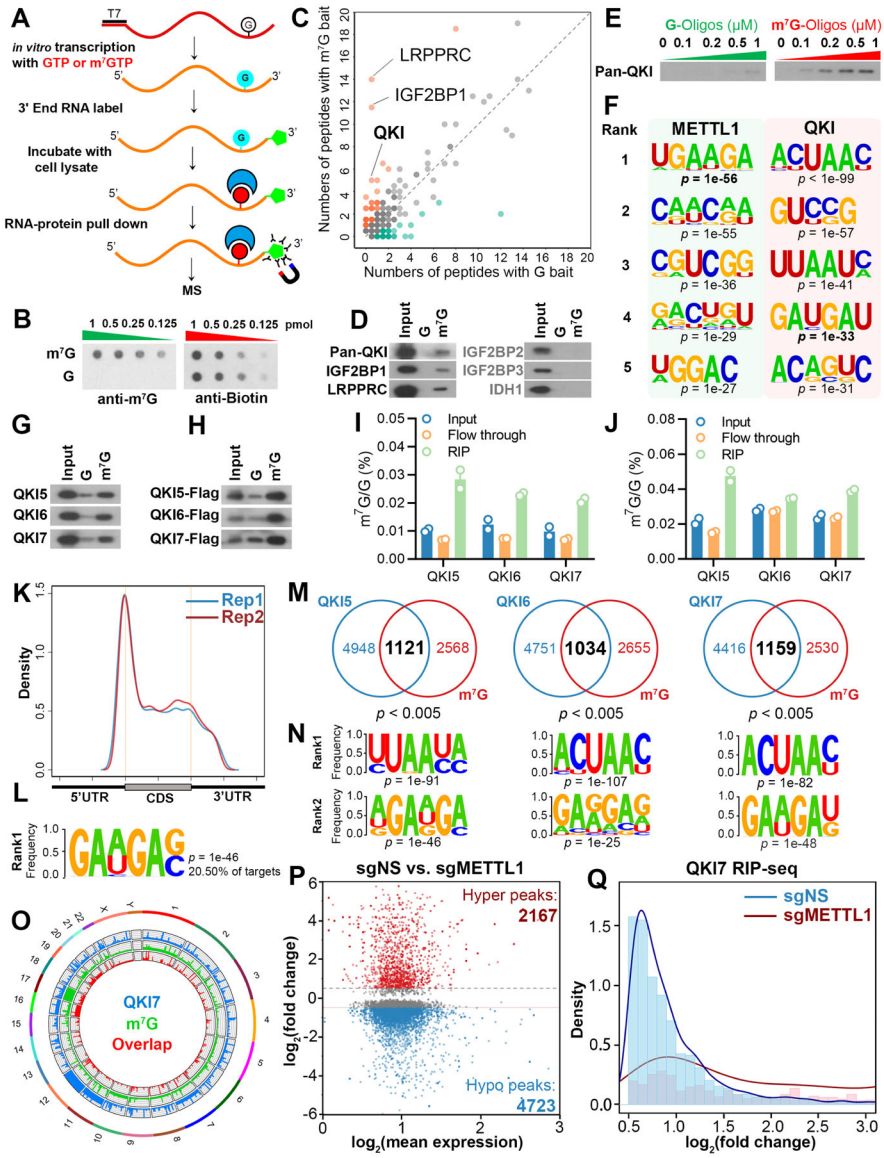

Figure 2. Selective binding of QKIs to internal m^{7}G residues in mRNA

(A) Schematic of RNA affinity chromatography and MS analysis.

(B) Dot blot showing the m^{7}G levels (left) and Biotin levels (right; loading controls) in the 60-mer m^{7}G/G ssRNA probes.

(C) Scatter plot of proteins bound to m^{7}G-Oligos versus G-Oligos as detected by the mass spectrometry.

(D) Western blotting showing the endogenous Pan-QKI, IGF2BP1-3, LRPPRC and IDH1 proteins pulled down by biotin-labeled G-Oligos and m^{7}G-Oligos from HepG2 whole cell lysates.

(E) RNA pulldown assays showing the dose-dependent interaction between endogenous Pan-QKI and biotin-labeled G-Oligos (left) or m^{7}G-Oligos (right).

(F) The top five binding motifs of METTL1 and QKI.

(G) Western blotting showing the cell-free binding between recombinant QKI proteins and biotin-labeled G-Oligos or m^7G-Oligos.
(H) Western blotting showing the flag-tagged QKI5, QKI6 and QKI7 proteins pulled down by biotin-labeled G-Oligos or m^7G-Oligos using whole cell lysates from QKI5-, QKI6-, and QKI7-overexpressing HeLa cells, respectively.
(I) Quantification of m^7G/G ratio by LC-MS/MS in decapped polyA$^+$ RNA bound by recombinant QKIs as determined by cell-free RIP assay (mean ± SEM; n = 2).
(J) Quantification of m^7G/G ratio by LC-MS/MS in decapped polyA$^+$ mRNA bound by QKIs in HEK293T cells as determined by the *ex vivo* RIP assay (mean ± SEM; n = 2).
(K) Metagene profile showing the distribution of m^7G peaks in HepG2 cells in two biological replicates along a normalized transcript composed of 5'UTR, CDS and 3'UTR.
(L) Top internal m^7G motif in HepG2 mRNAs, identified by HOMER.
(M) Overlap between m^7G-modified transcripts and QKI-bound transcripts in HepG2 cells.
(N) Top two motifs of the binding sites of QKI5 (left), QKI6 (middle) and QKI7 (right) in HepG2 cells, identified by HOMER.
(O) Circos plot showing the QKI7-binding peaks (blue), internal m^7G peaks (green), and overlapping peaks (red) in HepG2 cells.
(P) MA plots displaying the hyper (increased) and hypo (decreased) QKI7 binding peaks in HepG2 mRNAs upon *METTL1* KO.
(Q) The frequency distribution of QKI7 binding peaks in sgNS and sg*METTL1* HepG2.
See also Figure S2 and Table S2–3.

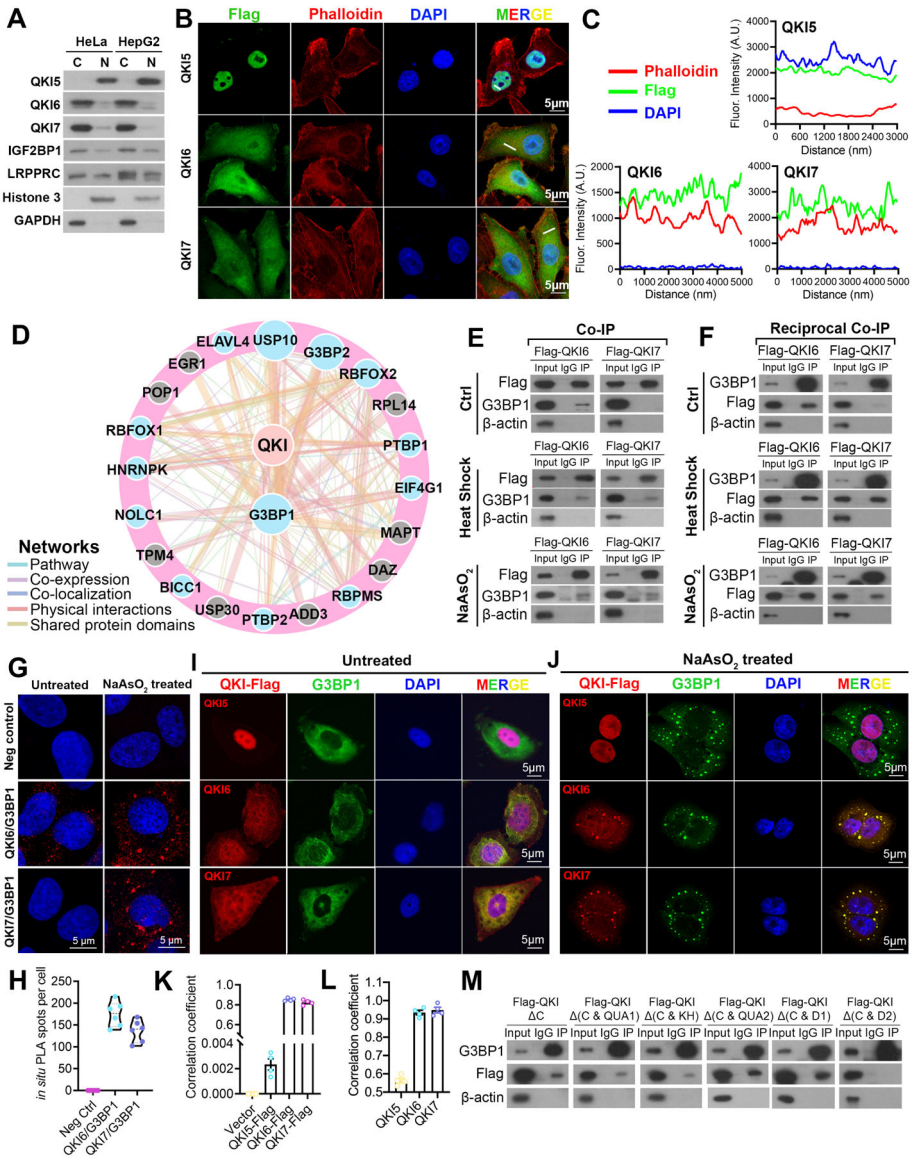

Figure 3. QKI proteins interact with SG core protein G3BP1 under stress conditions

(A) Subcellular localization of the potential m^{7}G binding proteins in HeLa and HepG2 cells (C = cytosol; N = nuclear).

(B) IF staining of ectopically expressed flag-tagged QKIs in HeLa cells.

(C) Profile intensity showing Flag/Phalloidin/DAPI fluorescence signals of the white lines in (B).

(D) The predicted interaction network of QKI binding proteins.

(E-F) Co-IP (E) and reciprocal Co-IP (F) showing the interaction between QKI6 (Flag) or QKI7 (Flag) and G3BP1 in HEK293T cells under normal (Ctrl) and stress conditions.

(G) *In situ* detection of QKI6-G3BP1 and QKI7-G3BP1 interaction via PLA in untreated (left) and $NaAsO_2$ treated (right) U2OS cells.

(H) Quantification of *in situ* PLA puncta in $NaAsO_2$-treated U2OS cells.

(I-J) IF staining of Flag-tagged QKIs and G3BP1 in U2OS cells under normal (I) or $NaAsO_2$-mediated stress (J) conditions.

(K-L) Pearson correlation analysis showing the colocalization of Flag-tagged QKIs with SGs (G3BP1) (K) or the RFP-tagged QKIs with G3BP1-GFP (L) in $NaAsO_2$-treated U2OS cells (mean ± SEM; n = 4).

(M) Co-IP showing the potential interaction between G3BP1 and several truncated QKIs in HEK293T cells under stress conditions.

See also Figure S3.

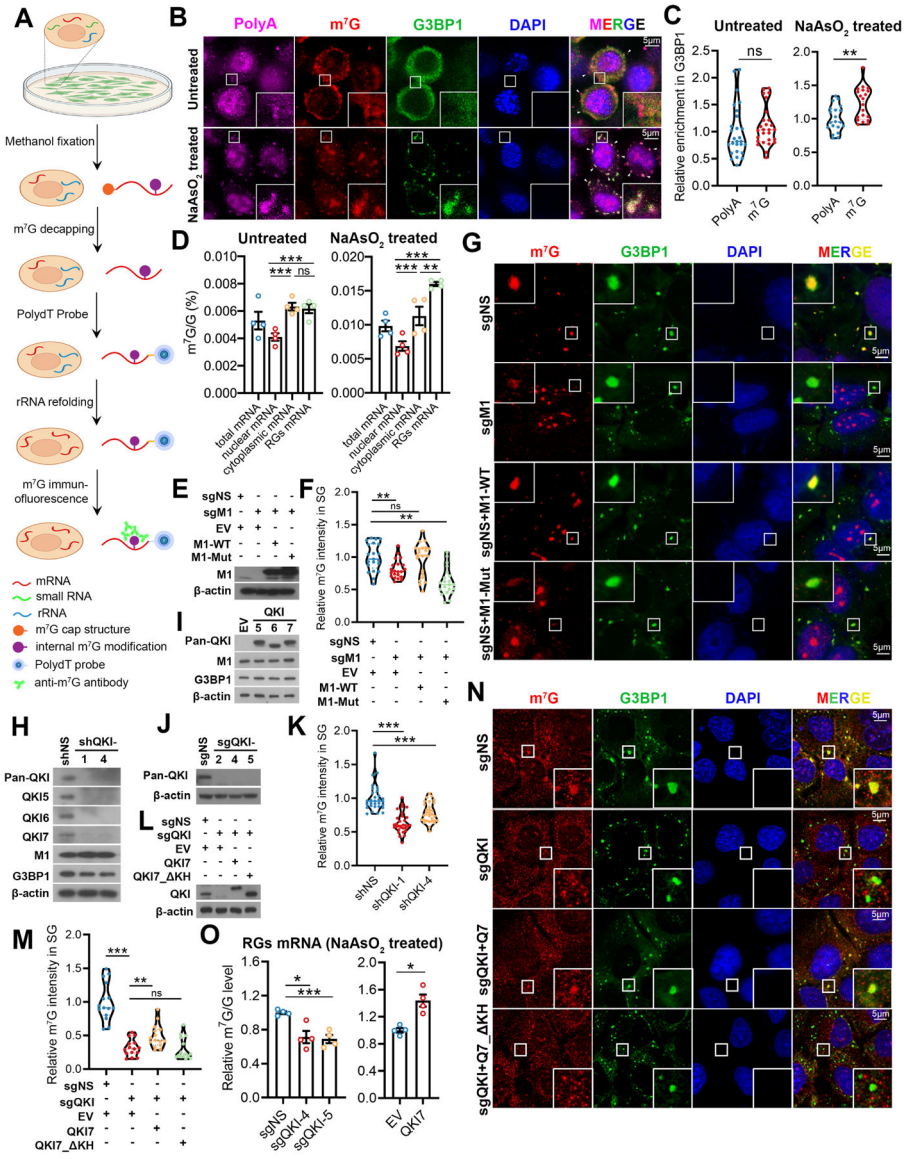

Figure 4. QKI transfers internal m^{7}G-decorated mRNAs into SGs

(A) Workflow for IF staining of internal m^{7}G-modified polyA$^+$ mRNA in adherent cells.

(B) IF staining of internal m^{7}G-modified mRNA in HeLa cells under normal and $NaAsO_2$-induced stress conditions.

(C) Relative enrichment of m^{7}G signal and polyA signal in SGs (G3BP1-positive dots) of HeLa cells with or without $NaAsO_2$ treatment.

(D) m^{7}G/G levels in cap-depleted total, nuclear, cytoplasmic, and insoluble RNA-granule (RG)-enriched polyA$^+$ mRNAs isolated from U2OS under normal and stress conditions (mean ± SEM; n = 4).

(E) Western blotting showing the level of wild-type or catalytic inactive mutant METTL1 in U2OS cells with *METTL1* KO.

(F-G) Violin plots (F) and representative IF pictures (G) of internal m^7G modification in $NaAsO_2$-treated U2OS cells with or without *METTL1* KO and rescued *METTL1* expression.

(H) Western blotting showing the level changes of indicated proteins in U2OS cells upon *QKI* KD.

(I-J) Western blotting showing the levels of indicated proteins in U2OS cells upon QKI overexpression (I) or KO (J).

(K) Relative fluorescence intensity of m^7G signals in SGs upon *QKI* KD in U2OS cells.

(L) Western blotting showing the rescued levels of wild-type and truncated (Δ KH domain) QKI7 in U2OS cells with *QKI* KO.

(M-N) Violin plots (M) and representative immunofluorescence pictures (N) of internal m^7G modification in $NaAsO_2$-treated U2OS cells with or without *QKI* KO and forced expression of wild-type or truncated QKI7.

(O) LC-MS/MS quantification of m^7G/G ratio in decapped insoluble RG-enriched $polyA^+$ mRNA fractions from $NaAsO_2$-treated U2OS cells upon *QKI7* KO (left) and overexpression (right) (mean ± SEM; n = 4).

Two-tailed student's t-test (C, K, and O); Two-way ANOVA (D, F, and M). ns, not significant; $*p < 0.05$; $**p < 0.01$; $***p < 0.001$.

See also Figure S4.

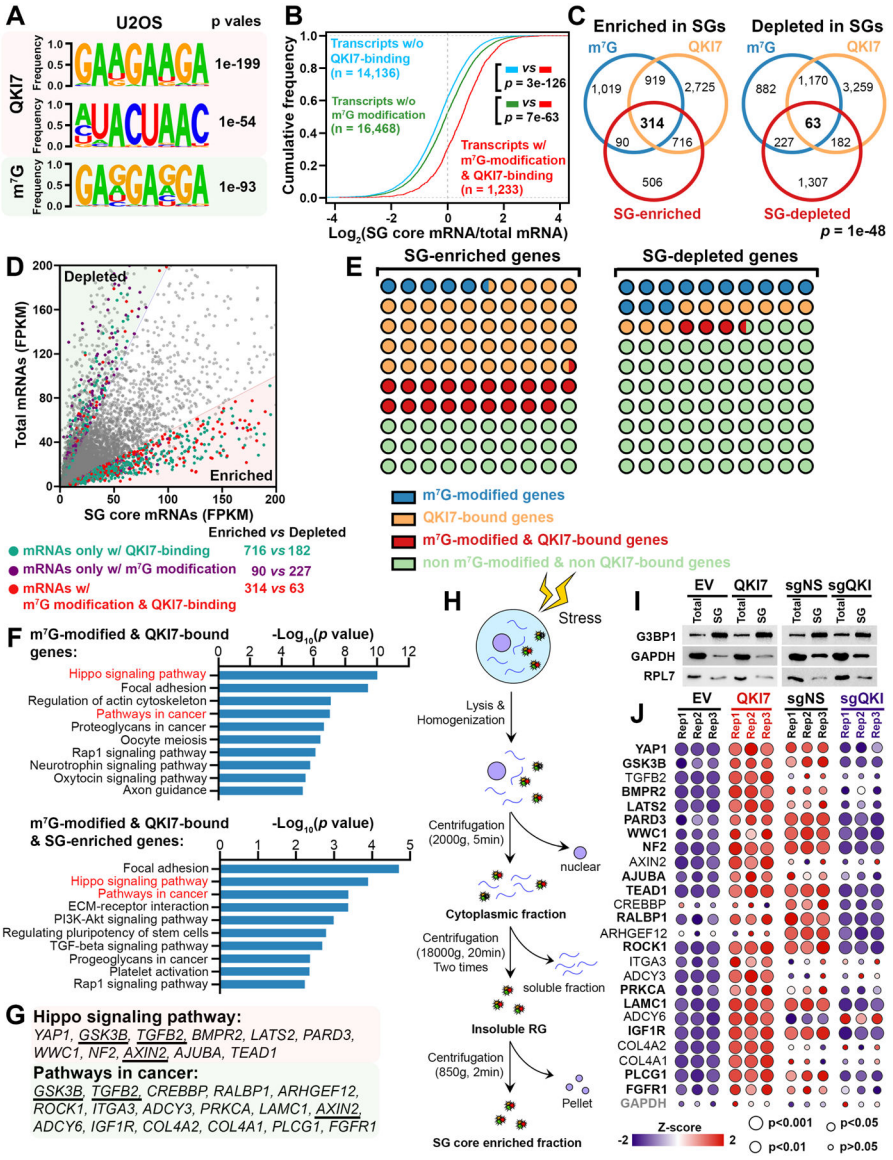

Figure 5. Transcriptome-wide analysis of QKI7-bound and internal m^{7}G-modified transcripts in SGs

(A) Motifs enriched in QKI7-binding peaks and internal m^{7}G peaks in U2OS cells.

(B) Cumulative distribution function (CDF) plot of mRNA enrichment in U2OS SGs.

(C) Overlap among internal m^{7}G-modified transcripts, QKI7-bound transcripts, and SG-enriched transcripts (left) or SG-depleted transcripts (right) in U2OS cells.

(D) Volcano diagram displaying the enrichment or depletion of SG-purified mRNAs compared to total mRNA.

(E) The mRNA composition of SG-enriched genes (left) or SG-depleted genes (right) in U2OS cells.

(F) KEGG pathway analysis of the internal m^{7}G-modified & QKI7-bound genes in U2OS entire transcriptome (top) or U2OS SG transcriptome (bottom).

(G) List of core-enriched genes in the “Hippo signaling pathway” and “pathway in cancer”.

(H) SG isolation workflow.

(I) Validation of efficient SG isolation from U2OS cells. G3BP1, GAPDH, and PRL7 were used as the marker of SG, cytoplasm, and ribosome, respectively.
(J) Heatmaps showing the relative abundance changes of the candidate target genes of QKI7 in SGs of U2OS cells upon *QKI7* overexpression (left, normalized to EV group) or KO (right, normalized to sgNS group) as determined by qRT-PCR. *GAPDH*, negative control.
Statistical analysis: Two-tailed student's t-test (B, J); Person's chi-square test (C).
See also Figure S5.

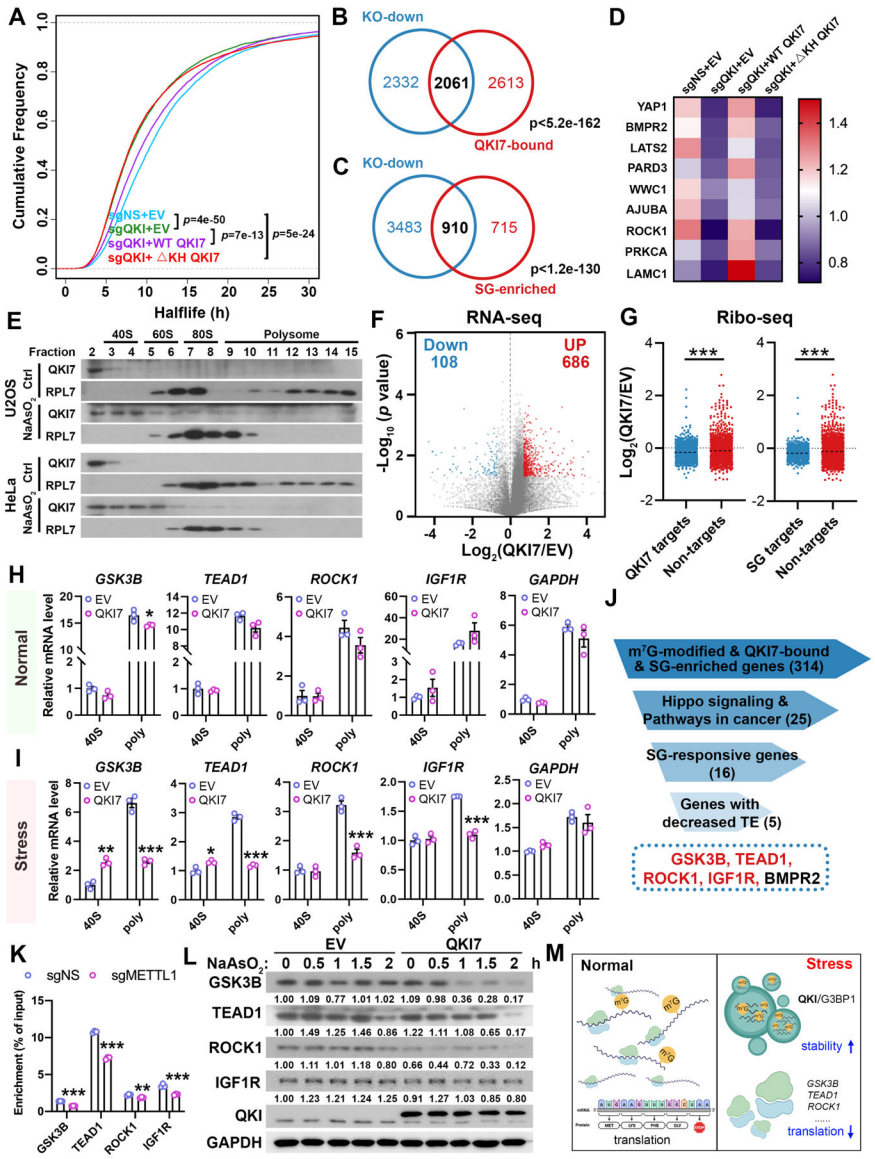

Figure 6. QKI7 regulates the metabolism of a set of its target transcripts in an internal m^{7}G-dependent manner

(A) CDF plot showing the effects of QKI level changes on global mRNA stabilities in $NaAsO_2$-treated U2OS cells.

(B-C) Overlap between transcripts with significantly decreased half-lives upon *QKI* KO ('KO-down') and QKI7-bound (B) or SG-enriched (C) transcripts in U2OS cells.

(D) Heatmap showing the relative half-life changes of the representative target genes in 0.2 mM $NaAsO_2$-treated U2OS cells with manipulation of QKI expression.

(E) Western blotting showing the distribution of QKI7 and RPL7 in 10%−50% sucrose gradient fractions of U2OS or HeLa cells under normal (ctrl) and stress conditions.

(F) Volcano diagram displaying the up-regulated and down-regulated genes in $NaAsO_2$-treated U2OS cells upon QKI7 overexpression.

(G) Scatter dot plot displaying the effect of QKI7 overexpression on translation efficiency of QKI7-bound (left) or SG-enriched (right) genes in U2OS cells under stress conditions.

(H-I) Distribution of representative targets in 40S fractions and polysome portions of U2OS cells upon QKI7 overexpression under normal (H) or $NaAsO_2$-treated (I) conditions (mean ± SEM; n = 3).

(J) Screening strategy for functionally essential targets of the QKI7-m^7G axis.

(K) QKI7-RIP qPCR showing the effects of *METTL1* KO on the enrichment of QKI7 on representative target mRNAs in U2OS cells (mean ± SEM; n = 3).

(L) Western blotting showing the levels of representative targets in control and QKI7-overexpressing U2OS cells upon $NaAsO_2$ treatment.

(M) Schematic illustration showing the effect of QKI on shuttling the internal m^7G-modified mRNA into SGs and regulating their translation efficiency and/or stability.

Two-tailed student's t-test (A, G, H, I, K); Hypergeometric test (B, C). *$p < 0.05$; **$p < 0.01$; ***$p < 0.001$.

See also Figure S6.

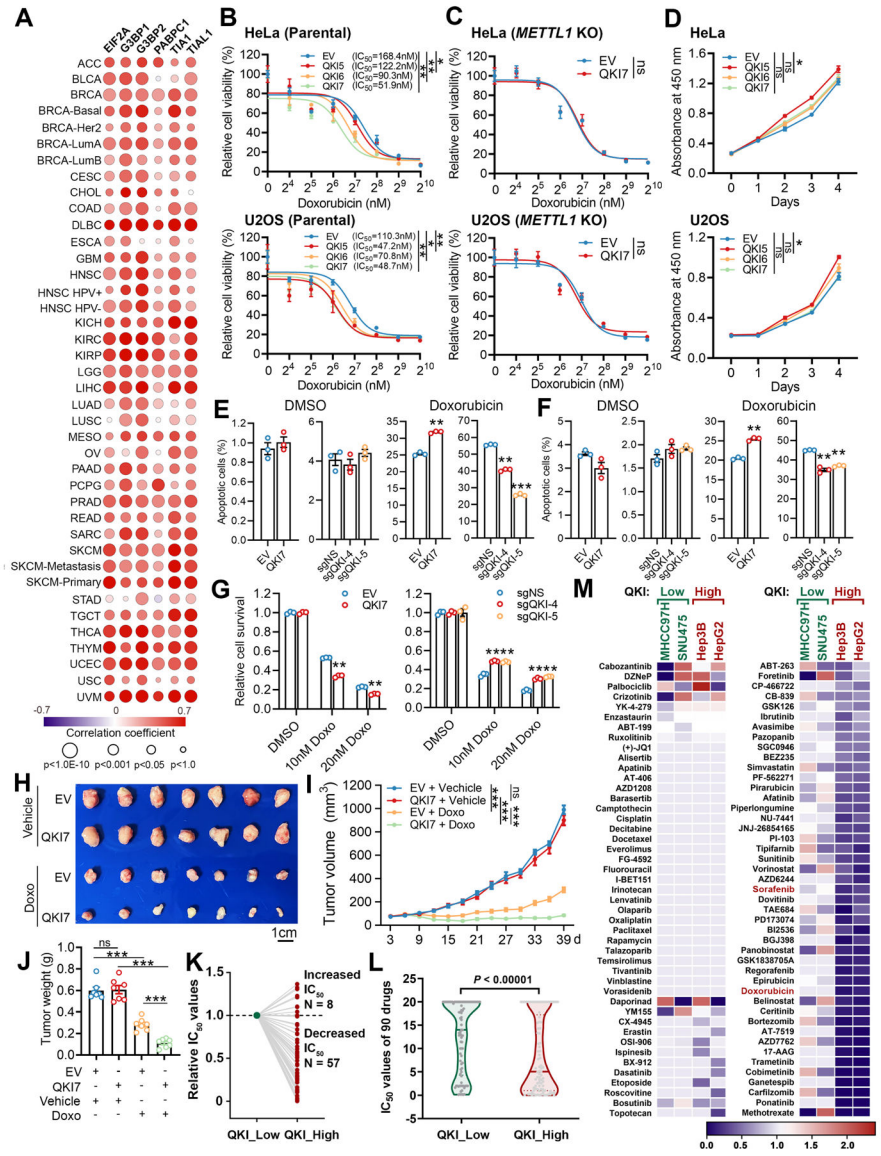

Figure 7. QKI confers sensitivity to chemotherapy drugs in cancer cells

(A) Correlation between *QKI* and SG core genes in various cancer types.

(B-C) Effect of *QKI* overexpression on doxorubicin IC_{50} in parental (B) or *METTL1* KO

(C) cancer cells.

(D) Effect of *QKI* overexpression on cancer cell proliferation.

(E-F) Effect of *QKI7* overexpression or *QKI* KO on the apoptosis of HeLa (E) or U2OS (F) cells treated with DMSO or doxorubicin for 24 hours.

(G) Clonogenic assay showing the effect of *QKI* overexpression (left) or KO (right) on survival of HeLa cells treated with DMSO or doxorubicin for 14 days.

(H) Images of xenografts formed by control or QKI7-overexpressing HeLa cells treated with doxorubicin (1 mg/kg) or vehicle.

(I-J) Tumor growth curve (I) and weight (J) from the indicated groups.

(K-L) Dot plots showing the relative (K) and exact (L) IC_{50} values of 90 drugs in QKI_Low and QKI_high HCC cell lines.

(M) Heatmap presenting the relative IC_{50} value of a variety of chemotherapy drugs in QKI_Low and QKI_High HCC cell lines.

Extra-sum-of-squares F test (B, C); One-way ANOVA (D, E, F); Two-way ANOVA (G, I, J); Two-tailed student's t-test (L). ns, not significant; *$p < 0.05$; **$p < 0.01$; ***$p < 0.001$. Data in B-G are presented as mean ± SEM (n = 3); data in I and J are presented as mean ± SEM (n = 7).

See also Figure S7.

KEY RESOURCES TABLE

REAGENT or RESOURCE	SOURCE	IDENTIFIER
Antibodies		
Anti-7-methylguanosine (m^7G) mAb	MBL International Corporation	Cat# RN017M, RRID: AB_2725740
Anti-N^6-methyladenosine (m^6A) antibody	Synaptic Systems	Cat# 202003, RRID: AB_2279214
METTL1 Polyclonal antibody	Proteintech	Cat# 14994-1-AP, RRID: AB_2142013
Anti-WDR4 Antibody (321.9)	Santa Cruz Biotechnology	Cat# sc-100894, RRID: AB_2288480
QKI Polyclonal antibody	Proteintech	Cat# 13169-1-AP, RRID: AB_2173138
Anti-QKI-5 Antibody	Bethyl Laboratories	Cat# A300-183A, RRID: AB_2173160
Anti-QKI-6 Antibody	Millipore	Cat# AB9906, RRID: AB_870987
Anti-QKI-7 Antibody	NIH NeuroMab Facility	Cat# N183/15, RRID: AB_2877379
G3BP1 polyclonal antibody	Proteintech	Cat# 13057-2-AP, RRID: AB_2232034
IMP1 (D33A2) Rabbit mAb	Cell Signaling Technology	Cat# 8482, RRID: AB_11179079
IMP2 (D4R2F) Rabbit mAb	Cell Signaling Technology	Cat# 14672, RRID: AB_2798563
IMP3 Antibody	Bethyl	Cat# A303-426A, RRID: AB_10951696
Anti-METTL3 antibody	Abcam	Cat# ab195352, RRID: AB_2721254
Anti-METTL14 antibody	Sigma-Aldrich	Cat# HPA038002, RRID: AB_10672401
IDH1 (D2H1) Rabbit mAb	Cell Signaling Technology	Cat# 8137, RRID: AB_10950504
LRPPRC Polyclonal antibody	Proteintech	Cat# 21175-1-AP, RRID: AB_10733879
VDAC1/2 Polyclonal antibody	Proteintech	Cat# 10866-1-AP, RRID: AB_2257153
Monoclonal ANTI-FLAG® M2 antibody	Sigma-Aldrich	Cat# F3165, RRID: AB_259529
HA tag Polyclonal antibody	Proteintech	Cat# 51064-2-AP, RRID: AB_11042321
RPL7 Polyclonal antibody	Proteintech	Cat# 14583-1-AP, RRID: AB_2254049
GSK3B Polyclonal antibody	Proteintech	Cat# 15113-1-AP, RRID: AB_10640527
TEAD1 Polyclonal antibody	Proteintech	Cat# 13283-1-AP, RRID: AB_2287290
ROCK1 Polyclonal antibody	Proteintech	Cat# 21850-1-AP, RRID: AB_10953526
IGF1R Polyclonal antibody	Proteintech	Cat# 20254-1-AP, RRID: AB_10667455
Anti-Puromycin Antibody	Millipore	Cat# MABE343, RRID: AB_2566826
GAPDH Monoclonal antibody	Proteintech	Cat# 60004-1-Ig, RRID: AB_2107436
Histone H3 (D1H2) XP® Rabbit mAb	Cell Signaling Technology	Cat# 4499, RRID: AB_10544537
β-Actin (8H10D10) Mouse mAb	Cell Signaling Technology	Cat# 3700, RRID: AB_2242334
Vinculin antibody (7F9)	Santa Cruz Biotechnology	Cat# sc-73614, RRID: AB_1131294
Goat Anti-Rabbit IgG H&L (HRP)	Abcam	Cat# ab6721, RRID: AB_955447
Goat Anti-Mouse IgG H&L (HRP)	Abcam	Cat# ab6789, RRID: AB_955439
Normal Mouse IgG control antibody	Millipore	Cat# 12-371; RRID: AB_145840
Normal Rabbit IgG control antibody	Millipore	Cat# 12-370, RRID: AB_145841
Streptavidin, Peroxidase Conjugate	Millipore	Cat# 189733-1ML
Anti-rabbit IgG (H+L), F(ab')2 Fragment (Alexa Fluor® 555 Conjugate)	Cell Signaling Technology	Cat# 4413, RRID: AB_10694110

REAGENT or RESOURCE	SOURCE	IDENTIFIER
Anti-mouse IgG (H+L), F(ab')2 Fragment (Alexa Fluor® 555 Conjugate)	Cell Signaling Technology	Cat# 4409, RRID: AB_1904022
Anti-rabbit IgG (H+L), F(ab')2 Fragment (Alexa Fluor® 488 Conjugate)	Cell Signaling Technology	Cat# 4412, RRID: AB_1904025
Anti-mouse IgG (H+L), F(ab')2 Fragment (Alexa Fluor® 488 Conjugate)	Cell Signaling Technology	Cat# 4408, RRID: AB_10694704
Anti-mouse IgG (H+L), F(ab')2 Fragment (Alexa Fluor® 647 Conjugate)	Cell Signaling Technology	Cat# 4410, RRID: AB_1904023
Phalloidin, CF555 Conjugate	Biotium	Cat# 00040-T
Bacterial and virus strains		
Stbl3 E. coli	Thermo Fisher Scientific	Cat# C737303
Chemicals, peptides, and recombinant proteins		
DMEM, High Glucose, with Pyruvate	GIBCO	Cat# 11995073
Penicillin Streptomycin	GIBCO	Cat# 15140122
PBS	GIBCO	Cat# 10010049
Trypsin-EDTA (0.05%)	GIBCO	Cat# 25300054
Fetal Bovine Serum	Omega Scientific	Cat# FB-01
β-mercaptoethanol	Thermo Fisher Scientific	Cat# 21985023
GlutaMax Supplement	Thermo Fisher Scientific	Cat# 35050061
Sodium Pyruvate	Thermo Fisher Scientific	Cat# 11360070
Plasmocin™ prophylactic	InvivoGene	Cat# ant-mpp
Puromycin	InvivoGene	Cat# ant-pr-1
Blasticidin	InvivoGene	Cat# ant-bl-1
Hygromycin B Gold	InvivoGene	Cat# ant-hg-5
Bovine Serum Albumin	Sigma-Aldrich	Cat# A2058
RIPA buffer	Sigma-Aldrich	Cat# R0278
Halt Phosphatase Inhibitor Cocktail	Thermo Fisher Scientific	Cat# 78420
Halt Protease Inhibitor Cocktail	Thermo Fisher Scientific	Cat# 78429
M-PER™ Mammalian Protein Extraction Reagent	Thermo Fisher Scientific	Cat# 78501
Pierce™ IP Lysis Buffer	Thermo Fisher Scientific	Cat# 87787
4×Laemmli Sample Buffer	Bio-Rad	Cat# 1610747
Pierce ECL Western Blotting Substrate	Thermo Fisher Scientific	Cat# PI32106
RiboLock RNase Inhibitor	Thermo Fisher Scientific	Cat# EO0382
SUPERase• In™ RNase Inhibitor	Thermo Fisher Scientific	Cat# AM2694
Pierce Protein A/G Magnetic Beads	Thermo Fisher Scientific	Cat# 88803
Pierce™ Anti-DYKDDDDK Magnetic Agarose	Thermo Fisher Scientific	Cat# A36797
Pierce™ 3x DYKDDDDK Peptide	Thermo Fisher Scientific	Cat# A36805
Nuclease-Free Water	Thermo Fisher Scientific	Cat# AM9937
QIAzol Lysis Reagent	Qiagen	Cat# 79306
Sodium Acetate (3M)	Thermo Fisher Scientific	Cat# AM9740

REAGENT or RESOURCE	SOURCE	IDENTIFIER
Glycogen	Thermo Fisher Scientific	Cat# R0551
Nuclease P1 from Penicillium citrinum	Sigma-Aldrich	Cat# N8630
Thermo Scientific FastAP Thermosensitive Alkaline Phosphatase	Thermo Fisher Scientific	Cat# EF0651
NEBNext® Magnesium RNA Fragmentation Module	New England Biolabs	Cat# E6150S
Tobacco Decapping Plus 2	Enzymax	Cat# 94
GTP	Sigma-Aldrich	Cat# G8877
m^7GTP	Sigma-Aldrich	Cat# M6133
Guanosine	Cayman Chemical Company	Cat# 27702
7-Methylguanosine	Cayman Chemical Company	Cat# 15988
Proteinase K, recombinant, PCR grade	Thermo Fisher Scientific	Cat# EO0491
DNase I, RNase-free	Thermo Fisher Scientific	Cat# EN0521
TURBO™ DNase	Thermo Fisher Scientific	Cat# AM2238
Micrococcal Nuclease	New England Biolabs	Cat# M0247S
RNase A/T1 mix	Thermo Fisher Scientific	Cat# EN0551
T4 polynucleotide kinase	New England Biolabs	Cat# M0201S
ATP	New England Biolabs	Cat#P0756S
Cycloheximide	Sigma-Aldrich	Cat# C4859
Sucrose	Sigma-Aldrich	Cat# S9378
Formamide	Sigma-Aldrich	Cat# F9037
Ponceau S	Sigma-Aldrich	Cat# P7170
Formaldehyde solution	Sigma-Aldrich	Cat# F8775
Crystal violet	Sigma-Aldrich	Cat# V5265
Permeabilization Buffer	Thermo Fisher Scientific	Cat# 00-8333-56
Duolink® In Situ PLA® Probe Anti-Rabbit PLUS, Affinity purified Donkey anti-Rabbit IgG (H+L)	Sigma-Aldrich	Cat# DUO92002
Duolink® In Situ PLA® Probe Anti-Mouse MINUS, Affinity purified Donkey anti-Mouse IgG (H+L)	Sigma-Aldrich	Cat# DUO92004
Duolink® In Situ Wash Buffers, Fluorescence	Sigma-Aldrich	Cat# DUO82049
Duolink® In Situ Detection Reagents Red	Sigma-Aldrich	Cat# DUO92008
Duolink® In Situ Mounting Medium with DAPI	Sigma-Aldrich	Cat# DUO82040
Stellaris® RNA FISH Hybridization Buffer	Biosearch Technologies	Cat# SMF-HB1-10
Stellaris® RNA FISH Wash Buffer A	Biosearch Technologies	Cat# SMF-WA1-60
Stellaris® RNA FISH Wash Buffer B	Biosearch Technologies	Cat# SMF-WB1-20
FastDigest NotI	Thermo Fisher Scientific	Cat# FD0595
FastDigest XbaI	Thermo Fisher Scientific	Cat# FD0684
FastDigest NheI	Thermo Fisher Scientific	Cat# FD0973
FastDigest BamHI	Thermo Fisher Scientific	Cat# FD0054
CloneAmp HiFi PCR Premix	Takara	Cat# 639298
DNA Ligation mix	Takara	Cat# 6023

REAGENT or RESOURCE	SOURCE	IDENTIFIER
Maxima SYBR Green qPCR Master Mix	Thermo Fisher Scientific	Cat# K0253
X-tremeGENE™ HP DNA Transfection Reagent	Sigma-Aldrich	Cat# 6366546001
Cell Counting Kit 8	Dojindo	Cat# CK04
Sodium Arsenite Solution	Millipore	Cat# 1.06277.1000
Actinomycin D	Sigma-Aldrich	Cat# A9415
Doxorubicin hydrochloride	Sigma-Aldrich	Cat# 44583
Sorafenib	Selleck Chemicals	Cat# S7397
Sodium borohydride	Sigma-Aldrich	Cat# 452882
Potassium borohydride	Sigma-Aldrich	Cat# 60080
Aniline	Sigma-Aldrich	Cat# 242284
Acetic acid	Fisher Scientific	Cat# BP1185-500
Streptavidin protein (HRP)	Abcam	Cat# ab7403
Amersham Hybond-N^+ membrane	Cytiva	Cat# RPN303B
Amersham ECL Prime Western Blotting Detection Reagent	Cytiva	Cat# RPN2232
Critical commercial assays		
mirVana™ miRNA Isolation Kit	Fisher Scientific	Cat# AM1560
Dynabeads™ mRNA Purification Kit	Thermo Fisher Scientific	Cat# 61006
Fisher BioReagents™ SurePrep™ Nuclear or Cytoplasmic RNA Purification Kit	Thermo Fisher Scientific	Cat# BP280550
Mitochondria Isolation Kit for Cultured Cells	Thermo Fisher Scientific	Cat# 89874
NE-PER™ Nuclear and Cytoplasmic Extraction Reagents	Thermo Fisher Scientific	Cat# 78835
RNA Clean & Concentrator-5	Zymo Research	Cat# R1015
Oligo Clean & Concentrator	Zymo Research	Cat# D4060
ZR small-RNA PAGE Recovery Kit	Zymo Research	Cat# R1070
Megashortscript™ T7 Transcription Kit	Thermo Fisher Scientific	Cat# AM1354
Pierce™ Magnetic RNA-Protein Pull-Down Kit	Thermo Fisher Scientific	Cat# 20164
Pierce™ RNA 3' End Biotinylation Kit	Thermo Fisher Scientific	Cat# 20160
APC Annexin V Apoptosis Detection Kit with PI	Biolegend	Cat# 640932
QuantiTect Rev. Transcription Kit	Qiagen	Cat# 205314
QIAprep Spin Miniprep Kit	Qiagen	Cat# 27104
QIAquick Gel Extraction Kit	Qiagen	Cat# 28704
PCR Mycoplasma Detection Kit	Applied Biological Materials	Cat# G238
In-Fusion® HD Cloning Plus CE	Takara	Cat# 638916
NEBNext small RNA Library Prep Kit	New England Biolabs	Cat# E7330S
NEBNext rRNA depletion kit	New England Biolabs	Cat# E6310S
KAPA Stranded mRNA-Seq Kit	Kapa Biosystems	Cat# 07962193001
NorthernMax™ Kit	Thermo Fisher Scientific	Cat# AM1940
Deposited data		
m^7G-seq (Raw and analyzed data)	This manuscript	GSE193039

REAGENT or RESOURCE	SOURCE	IDENTIFIER
RIP-seq (Raw and analyzed data)	This manuscript	GSE193039 and GSE218221
Ribo-seq (Raw and analyzed data)	This manuscript	GSE193039
mRNA stability profiling (Raw and analyzed data)	This manuscript	GSE218222
Experimental models: Cell lines		
HEK293T	ATCC	Cat# CRL-3216, RRID: CVCL_0063
HepG2	ATCC	Cat# HB-8065, RRID: CVCL_0027
Hela	ATCC	Cat# CCL-2, RRID: CVCL_0030
U-2 OS	ATCC	Cat# HTB-96, RRID: CVCL_0042
THLE-2	ATCC	Cat# CRL-2706, RRID: CVCL_3803
SNU475	ATCC	Cat# CRL-2236, RRID: CVCL_0497
Hep3B	ATCC	Cat# HB-8064, RRID: CVCL_0326
SNU449	ATCC	Cat# CRL-2234, RRID: CVCL_0454
Huh7	Dr. Wendong Huang (City of Hope, Duarte, CA)	N/A
MHCC97H	Dr. Wendong Huang (City of Hope, Duarte, CA)	N/A
Experimental models: Organisms/strains		
NOD.Cg-*Prkdc*^{scid}*Il2rg*^{tm1Wjl}/SzJ	The Jackson Laboratory	Cat# JAX:005557; RRID: IMSR_JAX:005557
Oligonucleotides		
Oligos for *in vitro* transcription	Integrated DNA Technologies	Table S1
Cy5-poly(dT)-LNA	Integrated DNA Technologies	N/A
Primers for qRT-PCR quantification	Integrated DNA Technologies	Table S1
Primers for plasmid construction	Integrated DNA Technologies	Table S1
Probe for Northern blotting	Integrated DNA Technologies	Table S1
Recombinant DNA		
pMIRNA1	This paper	N/A
pMIRNA1 3×Flag-METTL1	This paper	N/A
pMIRNA1 3×Flag-METTL1 EIR/AAA	This paper	N/A
pMIRNA1 HA-WDR4	This paper	N/A
pCDH-puro-cMyc (w/o GFP)	Cheng et al.[88]	Addgene plasmid # 46970; RRID: Addgene_46970
PCDH 3×Flag-METTL1 (w/o GFP)	This paper	N/A
PCDH 3×Flag-METTL1 EIR/AAA (w/o GFP)	This paper	N/A
PCDH 3×Flag-QKI5 (w/o GFP)	This paper	N/A
PCDH 3×Flag-QKI6 (w/o GFP)	This paper	N/A
PCDH 3×Flag-QKI7 (w/o GFP)	This paper	N/A
PCDH 3×Flag-QKI7 ΔKH (w/o GFP)	This paper	N/A
phage UbiC G3BP1-GFP-GFP	Wilbertz et al.[48]	Addgene plasmid # 119950; RRID: Addgene_119950
phage UbiC tagRFP-T-DDX6	Wilbertz et al.[48]	Addgene plasmid # 119947; RRID: Addgene_119947

REAGENT or RESOURCE	SOURCE	IDENTIFIER
lentiCas9-Blast	Sanjana et al.[89]	Addgene plasmid # 52962; RRID: Addgene_52962
lentiGuide-hygro	Stringer et al.[90]	Addgene plasmid # 104991; RRID: Addgene_104991
lentiGuide-hygro-sg*METTL1*-3	This paper	N/A
lentiGuide-hygro-sg*METTL1*-6	This paper	N/A
lentiGuide-hygro-sg*WDR4-4*	This paper	N/A
lentiGuide-hygro-*sgWDR4-5*	This paper	N/A
lentiGuide-hygro-sg*QKI-2*	This paper	N/A
lentiGuide-hygro-sg*QKI-4*	This paper	N/A
lentiGuide-hygro-sg*QKI-5*	This paper	N/A
pMD2.G	A gift from Dr. Didier Trono	Addgene plasmid # 12259; RRID: Addgene_12259
pMDLg/pRRE	Dull et al.[91]	Addgene plasmid # 12251; RRID: Addgene_12251
psPAX2	A gift from Dr. Didier Trono	Addgene plasmid # 12260; RRID: Addgene_12260
pLKO.1_shNS	Stewart et al.[92]	Addgene plasmid # 8453
pLKO.1_sh*QKI-1*	Sigma-Aldrich	Cat# TRCN0000233371
pLKO.1_sh*QKI-4*	Sigma-Aldrich	Cat# TRCN0000233374
Software and algorithms		
GraphPad Prism 8	GraphPad	https://www.graphpad.com/scientific-software/prism/
GelAnalyzer	Lazar Jr. and Lazar Sr.	http://www.gelanalyzer.com
Image J	ImageJ.org	http://imagej.org/
Zen Black	Zeiss	http://www.zeiss.com
Flow Jo	BD Biosciences	http://www.flowjo.com
Cutadapt	Martin[78]	https://cutadapt.readthedocs.io/en/stable/#
RSEM-1.2.31	Li and Dewey[80]	https://deweylab.github.io/RSEM/
STAR 2.7	Dobin et al.[79]	https://github.com/alexdobin/STAR
exomePeak-2.8.0	Meng et al.[81]	http://bioconductor.org/
HOMER	Heinz et al.[82]	http://homer.ucsd.edu/homer/ngs/rnaseq/
DAVID Bioinformatics Resources	Huang da et al.[86]	https://david.ncifcrf.gov/